Summer 7-29-2021

Nanozyme: A Developing Nanotechnology for the Detection of Foodborne Pathogens

Nilamben D. Panchal
Pittsburg State University, nilampd2510@gmail.com

`

NANOZYME: A DEVELOPING NANOTECHNOLOGY FOR THE DETECTION OF FOODBORNE PATHOGENS

A Thesis Submitted to the Graduate School
in Partial Fulfillment of the Requirements
for the Degree of
Master of Science in Polymer Chemistry

Nilamben Panchal

Pittsburg State University

Pittsburg, Kansas

July 2021

NANOZYME: A DEVELOPING NANOTECHNOLOGY FOR THE DETECTION OF FOODBORNE PATHOGENS

Nilamben Panchal

APPROVED:

Thesis Advisor _____
Dr. Santimukul Santra, Department of Chemistry

Committee Member _____
Dr. Irene Zegar, Department of Chemistry

Committee Member _____
Dr. Phillip Harries, Department of Biology

ACKNOWLEDGMENTS

First, I want to thank Dr. Santimukul Santra to giving me an opportunity to be part of his lab and this interesting research experience. According to my experience and interest, he designed such a good project for my thesis. His experience and guidance helped me a lot during my research and troubleshoot for the experiments.

I also want to thank the Department of Chemistry for providing such a good and supportive environment for research for international students.

My special thanks to Dr. Tuhina Banerjee for all her guidance and help throughout my research, her experience and knowledge in biochemistry and interest towards research helped me a lot. I am also thankful to all my Nanotheranostics lab members for supporting me in lab.

I extend my grateful thanks to Dr. Irene Zegar, Dr. James MacAfee, and Dr. Peter Chung gave me access to their lab facilities during the research.

I am grateful for having such supportive parents who gave me this education and this education experience abroad. My heartful thanks to Vinay, who was always there with me whenever I needed support. I also want thanks my sibling and relatives.

Finally, I want to thank my thesis committee members for their valuable time.

NANOZYME: A DEVELOPING NANOTECHNOLOGY FOR THE DETECTION OF FOODBORNE PATHPGENS.

An Abstract of the Thesis by
Nilamben Panchal

Growing foodborne infections have led to global health and economic burdens. *E. coli* O157:H7 is one of the most common disease-provoking pathogens and known to be lethal Shiga toxin-producing *E. coli* (STEC) strains. With a low infection dose in addition to person-to-person transmission, STEC infections are easily spread. As a result, specific and rapid testing methods to identify foodborne pathogens are urgently needed. Nanozymes have emerged as enzyme-mimetic nanoparticles, demonstrating intrinsic catalytic activity that could allow for rapid, specific and accurate pathogen identification in the agrifood industry. In this study, we explored a trimodal nanoplatform utilizing colorimetric kinetics based on the traditional ELISA assay with the synergistic properties of gold and iron oxide nanozymes, replacing the conventional horse radish peroxidase (HRP). We designed an easily interchangeable "ELISA sandwich" composed of a novel magneto-plasmonic nanosensor (MPnS) and with target antibodies (MPnS-Ab). Our experiments demonstrate a 100-fold increase in catalytic activity with the dual (magneto-plasmonic) nanozymes in comparison to HRP with observable color changes within 15 minutes. Results further indicate our MPnS-Ab is highly specific for *E. coli* O157:H7. As nanozymes display more stability than natural enzymes, tunable activity, and multi-functionality, our platform could provide a customizable, low-cost assay that combines high specificity with rapid detection for a variety of pathogens.

Table of Contents

LIST OF TABLES vii
LIST OF FIGURES viii
LIST OF ABBREVIATIONS x
Chapter I 1
Introduction 1
1. Background on *Escherichia coli* 1
1.1 Structure and Function 2
1.2 Classification 3
1.3 Habitat 4
1.4 Antigenic Structure 5
1.5 Serological Confirmation of *E. coli* O157:H7 6
1.6 Clinical Significance 6
1.7 *E. coli* in Food chain 7
1.8 Epidemiology: 8
2. Detection of *E. coli* 10
2.2 Conventional Methods 10
2.3 Immunological Detection Methods 12
2.4 PCR based detection method 13
2.5 Emerging Methods 15
Conclusion 18
Chapter II 19
Results and Discussion 19
1. Introduction 19
2. Results and Discussion 21
3. Characterization Studies of MPnS and MPnS Conjugates: 22
4. Characterization Studies of GNPs and IONPs: 25
5. Optimization Studies 27
6. Peroxidase-Like Catalytic Activity of Nanozymes 29
7. Optimization of concentration of detection antibody for stable conjugate assessment 31
8. Peroxidase-based Sandwich ELISA for the Detection of *E. coli* O157:H7 32
9. Specific and Rapid Detection of *E. coli* O157:H7 34
Chapter III 37
Experimental Section 37
1. Materials: 37
2. Instrumentations 37
3. Synthesis of Gold Nanoparticles (GNPs) 38
4. Synthesis of Iron Oxide Nanoparticles (IONPs) 38
5. Synthesis of Magneto Plasmonic Nanoparticles (MPnS) 38
6. Synthesis of MPnS-mAb 39
7. Bacterial Culture 39
8. Kinetic Analysis 40
9. Peroxidase like activity of nanozymes 40
10. Sandwich Immunoassay 40
11. Specificity Assay 41
12. Sandwich ELISA in real sample 41

Chapter IV 42
Conclusion and Future Study 42
References 43
Chapter I 43
Chapter II 47

LIST OF TABLES

Table 1. Stability of nanoparticles over 2 months of period in 1X PBS (pH 7.4). IONP stored at room temperature, GNP and MPnS stored at 4^{o} C……..27

Table 2: Kinetic parameters of IONPs, GNPs, MPnS and HRP nanozymes obtained from Michaelis-Menten curves……30

LIST OF FIGURES

Chapter I

Figure 1: Cell structure of *E. coli*……2

Figure 2: Phylogenetic tree of *Escherichia coli* O157:H7……..3

Figure 3: Types of flagella……..4

Figure 4: Antigenic structure of Enterobacteriaceae……...5

Figure 5: Cycle of events in spread of STEC. ……7

Figure 6: According to CDC number of outbreaks happened in last decade (2011-2020)……..…9

Figure 7: CT-SMAC plate after the incubation for 24 hours. Left side- colorless colonies *of E. coli* O157 STEC and right side- pink colonies of non O157 STEC……...……10

Figure 8: Procedure for isolation and identification of *E. coli* O157:H7…….……..11

Figure 9: *E. coli* O157:H7 using IMS enrichment method with Invitrogen Dynabeads MAX *E. coli* O157 and following acid (upper row) treatment of beads (down row)…….…..12

Figure 10: Schematic representation of the colorimetric detection of targeted antigen based on enzymatic activity of HRP for TMB oxidation…….…….13

Figure 11: Schematic representation of traditional PCR method……..14

Figure 12: Scheme of the lectin-based surface plasmon resonance biosensor for *E. coli* O157:H7 detection…….15

Figure 13: Detection of *E. coli* O157:H7 in PBS solvent using MFnS…….16

Figure 14: Detection of *E. coli* cells using aptamer conjugated AuNP-GO……..17

Figure 15. Schematic illustration of nanozyme-mediated ELISA. Synthesis of the magneto-plasmonic nanosensor (MPnS) and it's working principle for detection of *E. coli O157:H7*……20

Figure 16. Characterization of MPnS and antibody conjugated MPnS…….……23

Figure 17. Characterization of GNP and antibody conjugated GNP…….……24

Figure 18. Characterization of IONP and antibody conjugated IONP…….……25

Figure 19: Size of nanoparticles over a period of two months…….……26

Figure 20: Optimization of peroxidase-like activity of nanozymes and natural enzyme with (A) varied H_2O_2, (B) pH, (C) temperature and (D) hydrodynamic diameter…….28

Figure 21: Kinetic parameters of nanozymes and natural enzyme HRP exhibiting peroxidase activity: Steady state kinetic analysis using Michaelis-Menten Model of (A) HRP (B) GNPs (C) IONPs and (D) MPnS by varying TMB concentrations…….30

Figure 22: Flocculation curve of MPnS-MAb conjugates at varied MAb concentrations…….....31

Figure 23: Colorimetric and SPR detections of different CFUs of *E.coli O157:H7* spiked in 1X PBS using A) HRP, B) GNPs, C) IONPs, D) MPnS in conventional "sandwich ELISA" format……..32

Figure 24: Plot comparing the "sandwich ELISA" results using different nanozymes and natural enzyme HRP……33

Figure 25: Colorimetric detection of different CFUs of *E.coli O157:H7* spiked in (A) milk and (B) spinach rinse using MPnS in "sandwich ELISA" format……...…34

Figure 26: (A and B) Specificity of MPnS was evaluated by conducting MPnS-based sandwich ELISA in the presence of other bacterial cross-contaminants and a mixture. (C and D) Time-dependent *E. coli* O157:H7 detection assay using (A) HRP and (B) MPnS……35

LIST OF ABBREVIATIONS

ATCC:	American Type Culture Collection
AuNP:	Gold Nanoparticle
AuNP-GO:	Graphene Oxide coated Gold Nanoparticle
CDC:	Center of Disease Control
CFUs:	Colony Forming Units
Ct-SMAC:	Cexifime-potassium tellurite Sorbitol-MacConkey
DAEC:	Diffusely Adherent *Escherichia coli*
DLS:	Dynamic light scattering
EAEC:	*Enteroaggregative Escherichia coli*
EDC:	1-ethyl-3-(3-(dimethylamino) propylcarbodimide hydrochloride
EIEC:	*Enteroinvasive Escherichia coli*
ELISA:	Enzyme-linked Immunosorbent Assay
EPEC:	*Enteropathogenic Escherichia coli*
ETEC:	*Enterotoxigenic Escherichia coli*
FDA:	Food and Drug Administration
GI:	Gastrointestinal
GNP:	Gold Nanoparticle
GO:	Graphene Oxide
H_2O_2:	Hydrogen Peroxide
$HAuCl_4$:	Hydrogen tetrachloroaurate (III) hydrate
HC:	Hemorrhagic Colitis
HRP:	Horseradish Peroxidase
HUS:	Hemolytic Uremic Syndrome
IONP:	Iron oxide Nanoparticle
MFnS:	Magneto Fluorescent Nanosensor
MPnS:	Magneto-Plasmonic Nanosensor
NaCl:	Sodium Chloride
NHS:	*N*-hydroxysuccinimide
NM:	Nonmotile
OD:	Optical Density
PAA:	Polyacrylic Acid
PCR:	Polymerase Chain reaction

RT PCR:	Real-time Polymerase Chain reaction
SLT:	Shigalike Toxin
SMAC:	Sorbitol-MacConkey
SPR:	Surface Plasmon Resonance
STEC:	Shiga toxin producing *E. coli*
Stxs:	Shiga toxins
TMB:	3,3',5,5'-Tetramethylbenzidine
USDA-FSIS:	United States Department of Agriculture's Food Safety and Inspection Service
WHO:	World Health Organization

Chapter I

Introduction

Foodborne illness, also known as food poisoning, is caused by the consumption of food contaminated by bacteria or its toxin, viruses, chemicals, parasites, or other agents. Foodborne infection is a serious threat to human health worldwide. According to the Center of Disease Control (CDC), there are more than 250 foodborne diseases discovered by researchers and most of them are infections caused by different types of bacteria, parasites, and viruses. *Norovirus*, *Escherichia coli*, *Salmonella*, *Staphylococcus aureus*, *Vibrio*, *Campylobacter*, *Listeria*, *Clostridium perfringens*, *Clostridium botulinum* are some of the common foodborne germs.[1] Rapid and early detection of these pathogens is necessary to stop the outbreak of foodborne pathogens. According to the CDC, around 2,65,000 Shiga toxin producing *E. coli* (STEC) infections occur each year in the United States, and 36 % of those infections occur with STEC O157. The CDC estimated that around 3,600 hospitalizations and 30 deaths occur each year because of STEC infection.[2] *Escherichia coli* O157:H7 is a gram-negative, facultative anaerobic, rod-shaped bacteria. The cells are 1 µm X 2-6 µm in size and are capable of motion through peritrichous flagella (uniform distribution of flagella).[3] The pathogenic strains of *E. coli* which produces Shiga toxins (Stxs) causes bloody diarrhea, and around 5-10 % of infected people develop a life-threatening disease such as hemolytic uremic syndrome (HUS) and hemorrhagic colitis (HC).[4]

1. Background on *Escherichia coli*

E. coli is a gram-negative, facultative anaerobe, rod shaped bacteria, normally found in the intestines of humans and other warm-blooded animals.[5] In 1885, the German physician Theodor Escherich identified *Escherichia coli*.[6] In 1983, a Danish veterinarian discovered that the *E. coli* species includes different serotypes: some are pathogenic, and others are not.[7] *E. coli* appears in

the body of newborns within a few hours after the birth. There are more than 700 serotypes of *E. coli* based on polysaccharide and surface protein differences.[8]

1.1 Structure and Function

E. coli is a rod-shaped bacteria and the cell wall is multifaceted and thin (**Figure 1**).[9] The outer membrane is enclosed by a capsule structure which is made of polysaccharides. The cell wall is thick and composed of long filaments of glycans which are crosslinked with stretchable peptides which prevents the cell from lysis.[10] Periplasmic space is the space between the cell wall and plasma membrane. The cytoplasmic membrane controls the movement of molecules into and out of cells and it covers the cell fluid called cytoplasm.[11-12] Cytoplasm primarily contains DNA, RNA, phospholipids, proteins, glycogen, murein, lipopolysaccharides, metabolites, vitamins, certain inorganic ions, etc.[13] Ribosomes assist in the making of proteins. *E. coli* uses flagella for movement; these are made up of the basal body (rotary motor), the hook (universal joint) and the filament (helical propeller).[14] All these parts are composed of different proteins.[15]

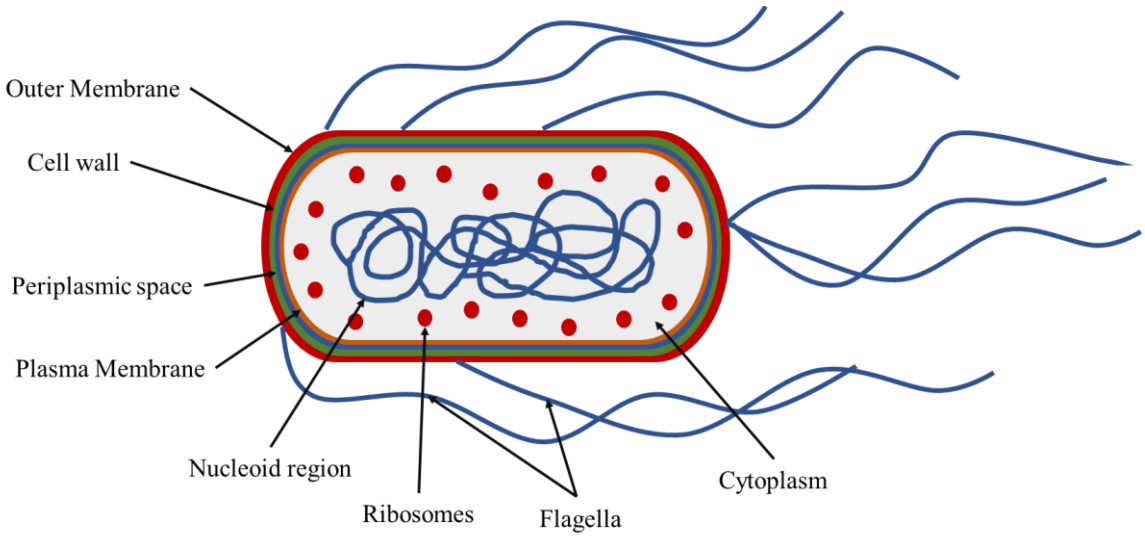

Figure 1: Cell structure of *E. coli*.

1.2 Classification

E. coli is a prokaryotic and unicellular organism which belongs to the kingdom of Bacteria because it does not have a nucleus or membrane bound organelles. *E. coli* is a gram-negative bacterium with the lipopolysaccharide membrane which comes under phylum Proteobacteria. *E. coli* is catagorized under class Gamma Proteobacteria beacause it is a facultative anaerobic gram-negative bacteria. *E. coli* is rod shaped which makes fall under Enterobacteriales (order). *E. coli* is a part of the Enterobacteriaceae family because it moves by petrichous flagella and it is an animal parasite. *E. coli* is mostly found in the mammalian gut and can be grown on soil and water, which allows it to fall under genus *Escherichia* (**Figure 2**). *Escherichia coli* O157:H7 have 157 somatic (O) antigens and 7 flagella (H) antigens.[16-18]

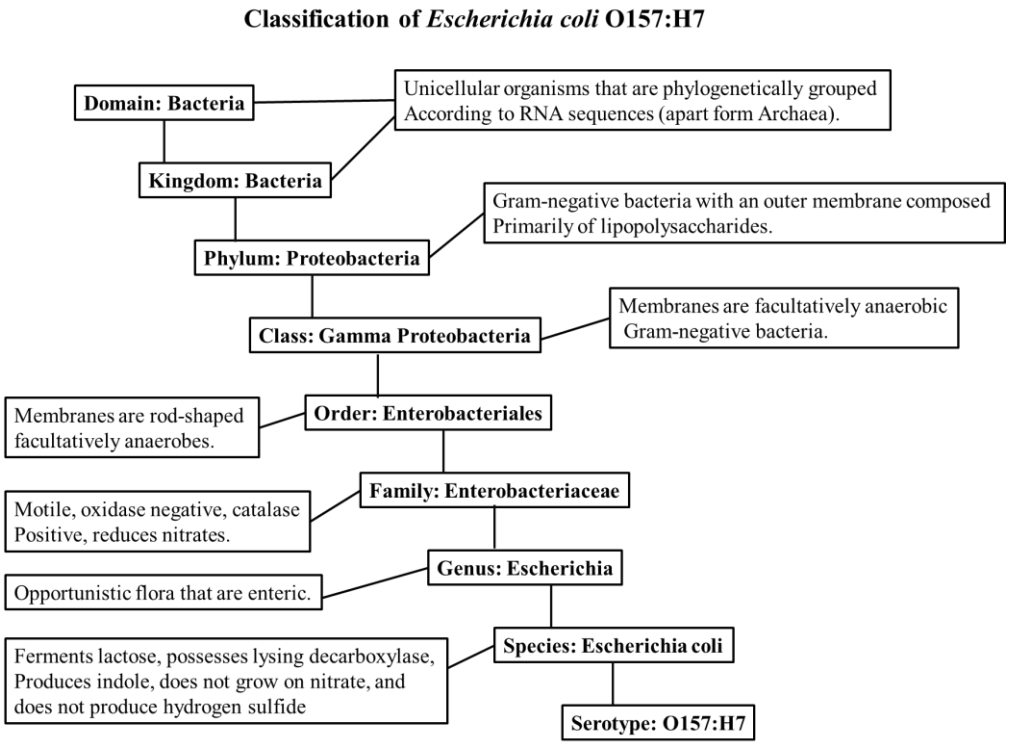

Figure 2: Phylogenetic tree of *Escherichia coli* O157:H7.[18]

1.3 Habitat

E. coli O157:H7 is mainly found in the gastrointestinal (GI) tract of most warm blood animals (cattle) and humans.[5] The human GI tract contains nearly 1 kg bacteria and almost 0.1-1% is *E. coli*. *E. coli* can be also found in contaminated water, food, sediments, and many other contaminated environments.[19] Cattle do not express the receptor which is specific for the verotoxin of *E. coli* O157:H7. Humans have this receptor, and when verotoxin binds to this receptor, it makes the host sick. In humans, *E. coli* O157:H7 is most commonly found in the GI tract in the colon. This provides a favorable environment to grow *E. coli* such as temperature, pH, and free food.[20]

The most favorable environments for *E. coli* are 37 ºC temperature and pH 7. However, environment is always changing, and *E. coli* have many ways to adapt the change. Based on two factors mutation and selective advantages, *E. coli* can adapt to changes in the environment and compete with other bacteria in the habitat. *E. coli* is a motile organism, and it can move with peritrichous flagella (**Figure 3**).[14] *E. coli* can sense any chemical changes in the environment and according to the chemical changes, it moves away from or towards the changes, which is known as chemotaxis.[21] For adaptation to changes in temperature and osmolarity in the environment, *E. coli* uses its ability to change the diameter of porins to capture the nutrients from the cell membrane. If there is a large nutrient molecule present in the habitat, *E. coli* will increase the diameter of porin in order to allow the molecule to enter in the cell. Conversely, if there is an inhibitory molecule present in the environment the diameter of porin will decrease and will prevent the molecule from entering the cell.[19]

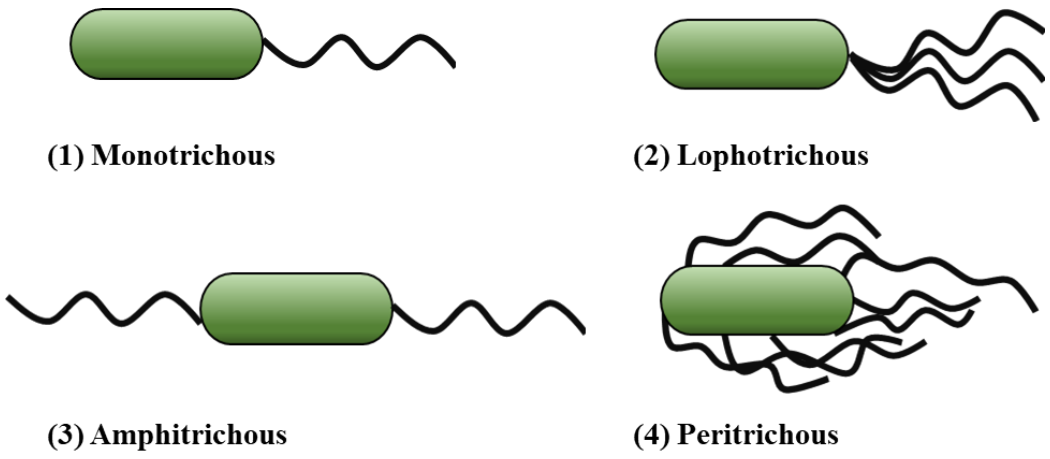

Figure 3: Types of flagella

1.4 Antigenic Structure

Antigenic typing or serotyping is generally based on three antigens somatic (O) antigen, flagellar (H) antigen, and capsular (K) antigen (**Figure 4**).[22] The somatic antigen is the polysaccharide part of the outer membrane. There are 186 types of O antigens that have been identified.[23] This antigen is heat resistant and stable up to 80-100 ^{o}C. It shows endotoxin activity because of lipid A fraction. O antigenic epitopes comprises the amino sugars and carbohydrate residues. These antigens are represented by numbers. H antigen is the protein flagellin which makes the strands of bacterial flagella. This protein is heat sensitive and can be denatured above 56 ^{o}C. Approximately 53 types of H antigens have been recognized.[23] In general, capsular antigens are composed of acidic polysaccharides and there are 80 types of K antigens.[24] This antigen is categorized into two groups: thermostable (I), and thermolabile (II). Most E. coli are identified by their O and H antigens only.[26] Isolates associated with diarrheal disease is limited, and identification of the O and H antigens of *E. coli* species is especially beneficial in epidemiologic investigations. For well-considered outbreaks with unidentified cause, the state health department sends the isolates to the CDC for further investigation.[27]

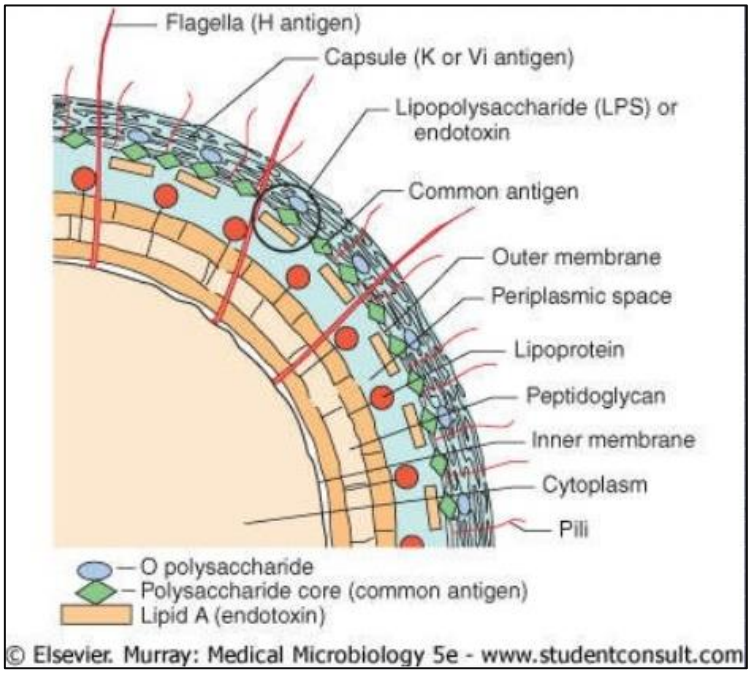

Figure 4: Antigenic structure of Enterobacteriaceae.[25]

1.5 Serological Confirmation of *E. coli* O157:H7

Detection of H7 flagellar antigen is require for the verification of *E. coli* O157:H7. H7- specific latex reagents and antisera are commercially accessible, but confirmation of H7 antigen frequently involves multiple phases.[28] Isolates that are H7 antigen negative or non-motile are tested for the Shiga toxin producing gene sequences. Almost 85% of O157 isolates from patients collected by the CDC are O157:H7 serotype, 12% are nonmotile (NM), and 3% are H types apart from H7.[27] *E. coli* O157:NM serotype often produces Shiga toxin, and those that are negative for Shiga toxin have a similar *fliC* restriction profile to *E. coli* O157:H7.[29] From human illness, no O157 strain with H antigen other that H7 has been discovered that produces the Shiga toxin.[27]

1.6 Clinical Significance

Pathogenic *E. coli* strains are categorized in two groups: diarrheagenic or intestinal *E. coli* and extraintestinal pathogenic *E. coli*. Diarrheagenic strains are grouped in five categories: STEC, *Enterotoxigenic Escherichia coli* (ETEC), *Enteropathogenic Escherichia coli* (EPEC), *Enteroaggregative Escherichia coli* (EAEC) and *Enteroinvasive Escherichia coli* (EIEC). The clinical significance of DAEC (Diffusely Adherent E. coli) is still uncertain. STEC is categorized under diarrheagenic *E. coli* corresponding to the production of toxins produced by this strain. The genetic material which causes hemolytic uremic syndrome and hemorrhagic colitis is unclear. The *E. coli* strains O157:H7 and O157:NM (nonmotile) are capable of producing one or more Shiga toxins, also known as verocytotoxins and are more frequently isolated in the presence of food borne disease outbreak.[27] In United States, nearly 185,500 cases of infections caused by O157:H7 strain are reported each year.[30]

E. coli O157:H7 and other STEC serotypes cause illness that results in mild nonbloody diarrhea, HUS, or severe bloody diarrhea (hemorrhagic colitis). Infection caused by the *E. coli* O157:H7 serotype has additional symptoms such as lack of high fever and abdominal cramps. According to CDC factsheet, nearly 5-10 % patients with STEC infections produce HUS.[31] In developing countries, the common cause for bloody diarrhea is the O157 STEC strain, and in North America it causes at least 80% cases of HUS. The incidence of isolation of O157 STEC from fecal specimens in the United States is greatest in the Northern Tier states. Serotype O157 STEC significantly

colonizes beef cattle, and thus ground beef has produced more O157 STEC epidemics than any other vehicle of transmission. According to CDC outbreaks, romaine lettuce, raw vegetables, frozen food, butter, and sprouts are the recognized vehicles of transmission. Raw milk, apple cider, unchlorinated municipal water, and roast beef are other identified vehicles of transmission. The other cause of transmission of O157 STEC is person to person contact because the minimal infective dose is very low (< 200 colony forming units (CFUs)). Outbreaks caused by person-to-person contact have appeared in families, schools, day care facilities, and long-term care institutions.[32]

1.7 *E. coli* in Food chain

As discussed above, the principal habitat of *E. coli* is the gut of warm-blooded animals mainly cattle.[5] *E. coli* is spread to humans principally through contaminated foods, such as raw milk, undercooked meat products, raw vegetables, and many more.[32] Fecal contamination of water includes animal manure, wastewater treatment, and on-site septic system. Contamination of food

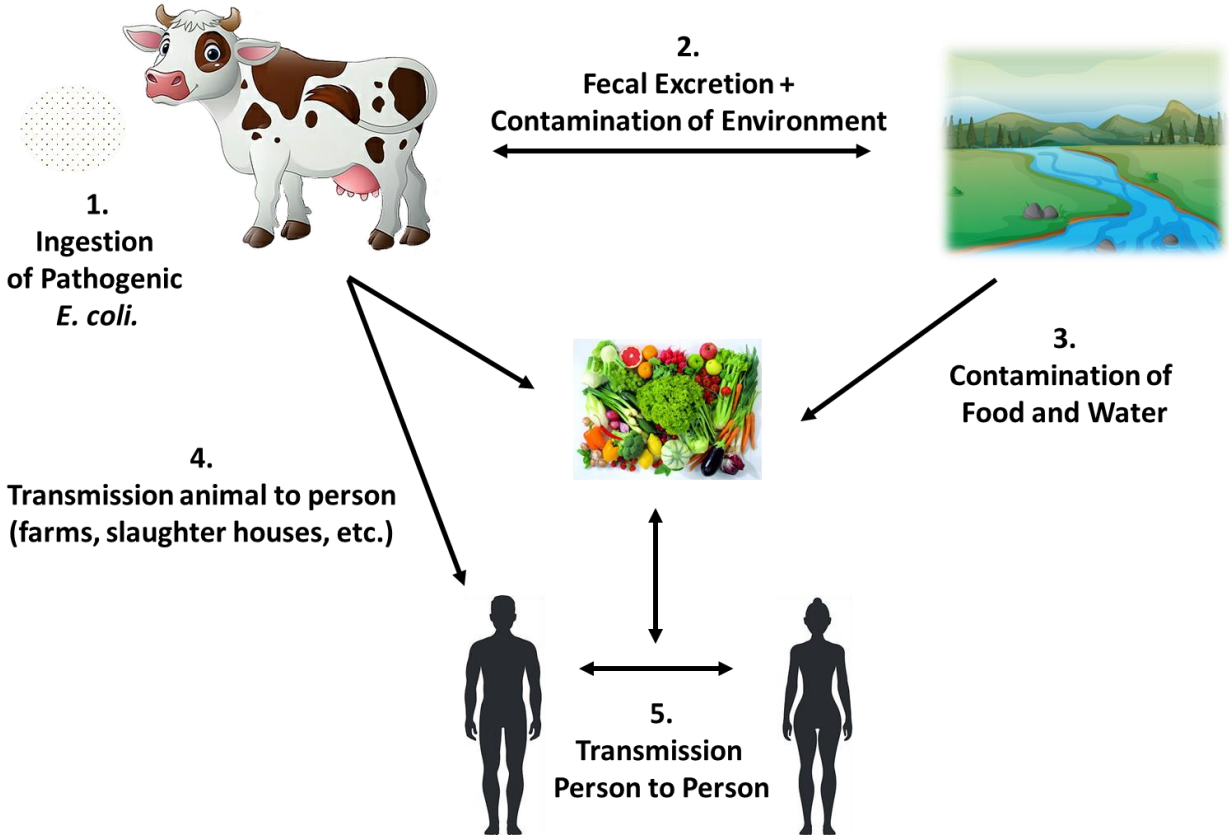

Figure 5: Cycle of events in spread of STEC.

occurs through contaminated water and cross contamination through food production.[32] Jimmy John's restaurant ready to eat salad (33 cases, 2013), Farm Rich frozen food (35 cases, 2013), Costco Rotisserie chicken salad (19 cases, 2015), Chipotle (55 cases, 2015), soynut butter (32 cases, 2017), Adam Bros farming (62 cases, 2018), romaine lettuce (167 cases, 2019), ground beef (209 cases, 2019) are some examples of *E. coli* outbreaks caused by food contamination in the United States in past decade.[34] The infectious *E. coli* are defecated in the excrement of either healthy or unhealthy hosts. The huge dissemination of animal and human waste into the environment results in a favorable habitat for the bacteria. For example, pathogens can be found in sewage, farm, animal manure, birds, wild animals, livestock, manure amended soil, and contaminated water.[32]

E. coli discharged into the environment by humans and animals through their waste may enter agriculture eco-systems through irrigation water, manure, contaminated seeds, nematode vectors, or insect pests and wildlife (**Figure 5**). Subsequently, contaminated fresh vegetables are also one of the main causes of *E. coli* outbreaks and resulted in approximately 11 outbreaks with more than 500 cases from different states in the United States. *E. coli* can survive in contaminated soil for almost 20 months, and therefore may remain as an environmental contaminant for an extended period. Moreover, *E. coli* survives on crop roots and leaves much longer than in soil. Younger leaves provide better habitat than older leaves, and damaged leaves, leaves with better quantities of nitrogen, and fruits are capable of supporting faster reproduction and increased survival of *E. coli.*[34] Recently, foodborne illness outbreaks correlated with raw vegetable sprouts has increased concerns among consumers and public health agencies. In 2020, in the United States, there was a *E. coli* outbreak because of clover sprouts (51 cases).[33]

1.8 Epidemiology:

In the United States, an approximate 73,480 cases due to *E. coli* O157 disease occur each year, leading to an approximate 61 deaths and 2,168 hospitalizations annually. In 1993, after a multistate outbreak of *E. coli* O157 associated with undercooked ground beef patties from restaurant chain, *E. coli* O157 became largely acknowledged as a threatening and important pathogen. *E. coli* O157 became a nationally notifiable disease in 1994, and by 2000, reporting was mandatory in 48 states.[31] The largest *E. coli* O157 outbreak associated with ground beef in 1994 reported in 4 states, includes more than 700 cases and mostly children, 53 peoples developed HUS, and 4 children died. The outbreak was related to undercooked beef from a restaurant. In 1999, the CDC reported the largest *E. coli* O157 outbreak in the United States, linked to contaminated drinking water that caused 781

cases, 15 developed HUS, and there were 2 deaths. The associated water was from a short term uncontrolled well at a fairground. An adequate amount of chlorine and a properly functioning water system can prevent *E. coli* O157 infection from drinking water.[31]

In 2006, an *E. coli* O157 outbreak linked to fresh spinach caused 199 illnesses in 26 states, including 102 hospitalizations; 31 people developed HUS, 22 children became ill, and 3 deaths were reported. The health departments, CDC, and United States Department of Agriculture's Food Safety and Inspection Service (USDA-FSIS) investigated a multistate *E. coli* O157 outbreak and recalled 21.7 million pounds of Topp's brand frozen ground beef patties. Again in 2009, CDC and USDA-FSIS reported recall of 545,699 pounds of Fairbank Farm's ground beef contaminated with *E. coli* O157:H7.[33]

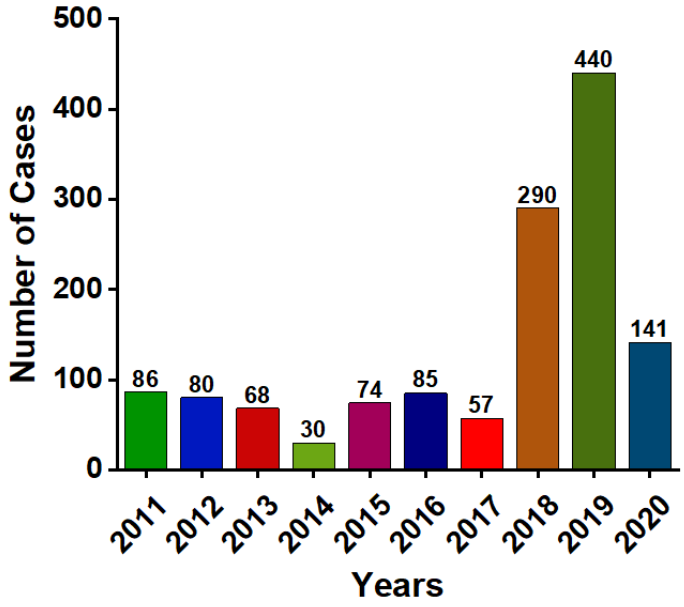

Figure 6: According CDC number of cases happened in last decade (2011-2020).[33]

2. Detection of *E. coli*

2.2 Conventional Methods

Conventional methods for detection of *E.* coli include culturing, plating and biochemical tests. The detection of *E. coli* O157:H7 can be carried out using sorbitol-MacConkey (SMAC) agar which consist of a carbohydrate, bile salt, indicator, and sorbitol.[34-35] To increase the sensitivity, cexifime and potassium tellurite added to SMAC agar (Ct-SMAC).[36] After overnight incubation of the sample on SMAC agar, colorless colonies (sorbitol negative) indicate the presence of O157:H7, which does not ferment sorbitol and pink colonies (sorbitol positive) shows the presence of other Enterobacteriaceae (**Figure 7**). Suspected *E. coli* colonies are selected and inoculated into identification media (Klinger's Iron agar, Triple Sugar Iron agar).[37]

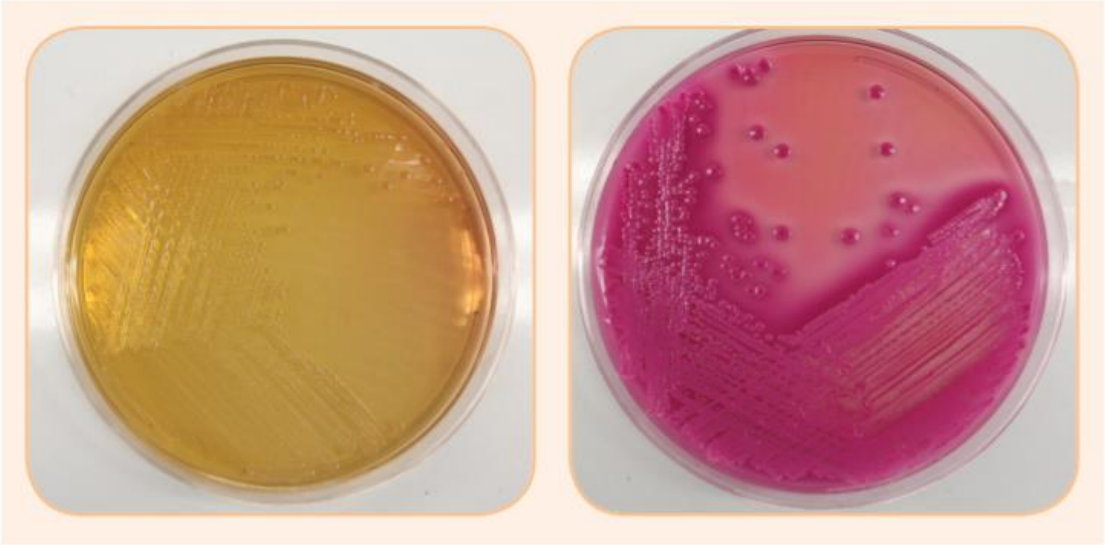

Figure 7: CT-SMAC plate after the incubation for 24 hours. Left side- colorless colonies of *E. coli* O157 STEC and right side- pink colonies of non O157 STEC.[38]

Even though sorbitol negative *E. coli* O157 is prominent, sorbitol positive *E. coli* O157 (non-motile) has appeared as a cause of HUS in the Australia and Europe. This isolate will not be identified on SMAC as they produce pink colonies like other Enterobacteriaceae. Additionally, the potassium tellurite included in CT-SMAC can inhibit the growth of sorbitol fermenting *E. coli* O157. Hence, the sorbitol positive colonies should be further examined for O157.[36]

Isolation and identification of *E. coli* using conventional methods have limitations such as the long duration of time required (1-7 days) and the labor-intensive process.[34]

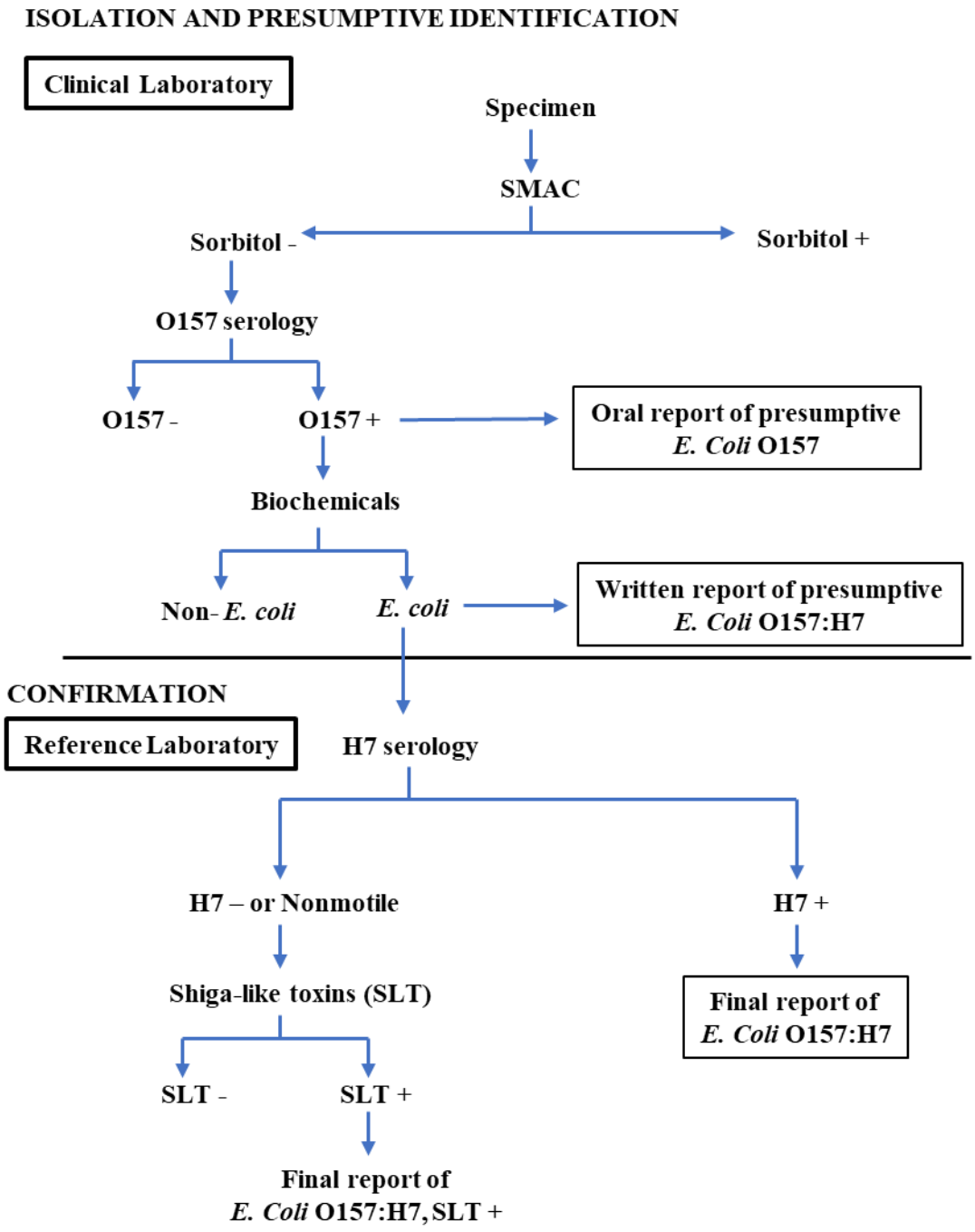

Figure 8: Procedure for isolation and identification of *E. coli* O157:H7.[40]

Immunomagnetic Separation:

A food sample containing *E. coli* O157:H7 with other micro flora, platting is ineffective without a pre-enrichment step. Immunomagnetic separation is the procedure to isolate the specific bacteria from a mixed culture using superparamagnetic beads (they show magnetic property only in the occurrence of an outside magnetic field) covered with pathogen specific antibodies to isolate the target bacteria from other microflora and food matrices. The most frequent carrier is Dynabeads which consist of polystyrene-based particles in sizes ranging from 2.8 to 4.5 µm.[35]

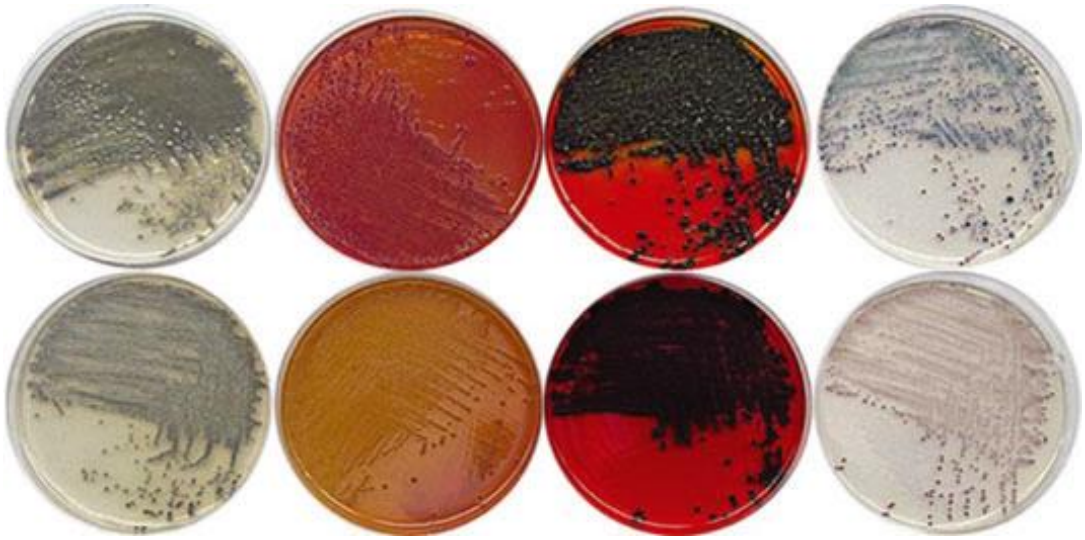

Figure 9: Recovery of *E. coli* O157:H7 using IMS enrichment method with Invitrogen Dynabeads MAX *E. coli* O157 (upper row) and following acid treatment of beads (down row). Different selective media used for the recovery of *E. coli* O157:H7.[41]

2.3 Immunological Detection Methods

Immunological detection methods are widely used for the detection of *E. coli* O157:H7, because of their sensitivity and specificity.[35]

2.3.1 Enzyme-linked Immunosorbent Assay (ELISA)

ELISA, which is simple, fast, cheap, and plate-based assay, and widely used in clinical analyses and laboratories for the detection of target analytes.[42] Enzymes are biological catalysts that

accelerates chemical reactions, which act on substrates and make a product (TMB oxidation) (**Figure 10**).[43] The well plate is coated with capture antibody which binds with the specific target analyte or antigen. The enzyme labelled detection antibody binds with the analyte. Finally, addition of enzyme specific substrate gives colored product which observed via naked eye. However, there is one limitation this conventional ELISA using enzyme-antibody conjugates as labels has relatively low sensitivity.[44] To overcome this issue, different methods have been developed; Malou and Raoult combined the ELISA with PCR assay to improve the sensitivity of the assay; Gould et. al., introduced biotin-streptavidin system; Chen and his group developed the technique of enzyme loaded nanoparticles.[45-47]

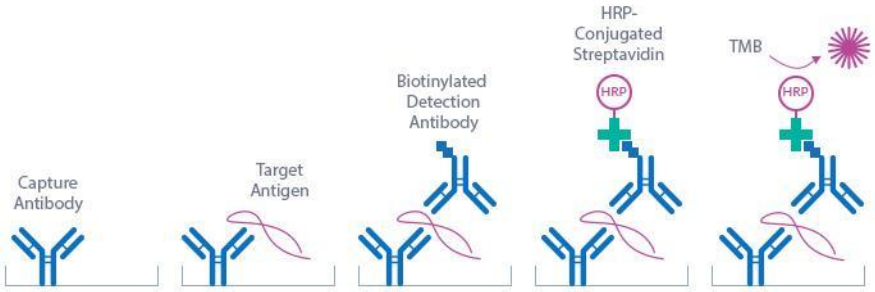

Figure 10: Schematic representation of the colorimetric detection of targeted antigen based on enzymatic activity of HRP for TMB oxidation.

Traditional ELISA uses horseradish peroxidase (HRP) enzyme, but these enzymes have limited catalytic activity to environmental conditions, high-cost demand, and low stability (denaturation and digestion). To overcome these limitations researchers have developed nanosensors which have similar catalytic properties and can be used as HRP mimic.[48]

2.4 PCR based detection method

PCR-based detection methods are widely used for the detection of foodborne pathogens. In the PCR method, the repeated cycles make millions of copies of the targeted DNA sequences in just a few hours. However, there is one main disadvantage of this method, which is that these repeated cycles can amplify the dead cells, so it requires trained individual for experiment.[35] PCR requires a thermal cycling instrument, and one cycle is comprised of the following three steps (**Figure 11**):

1. Denaturation: This step is performed under high temperature at 95° C for 1 minute for the separation of double stranded DNA helix.
2. Annealing: This step is carried out at lower temperature 40-60° C; it allows the primers to attach to complementary nucleotides of the targeted DNA sequence.
3. Extension: This phase is carried out at 72 °C to allow the DNA polymerase enzyme to operate optimally in the extension of the primers by adding one suitable nucleotide after another, resulting in the formation of a DNA complementary strand to the desired DNA sequence.[49]

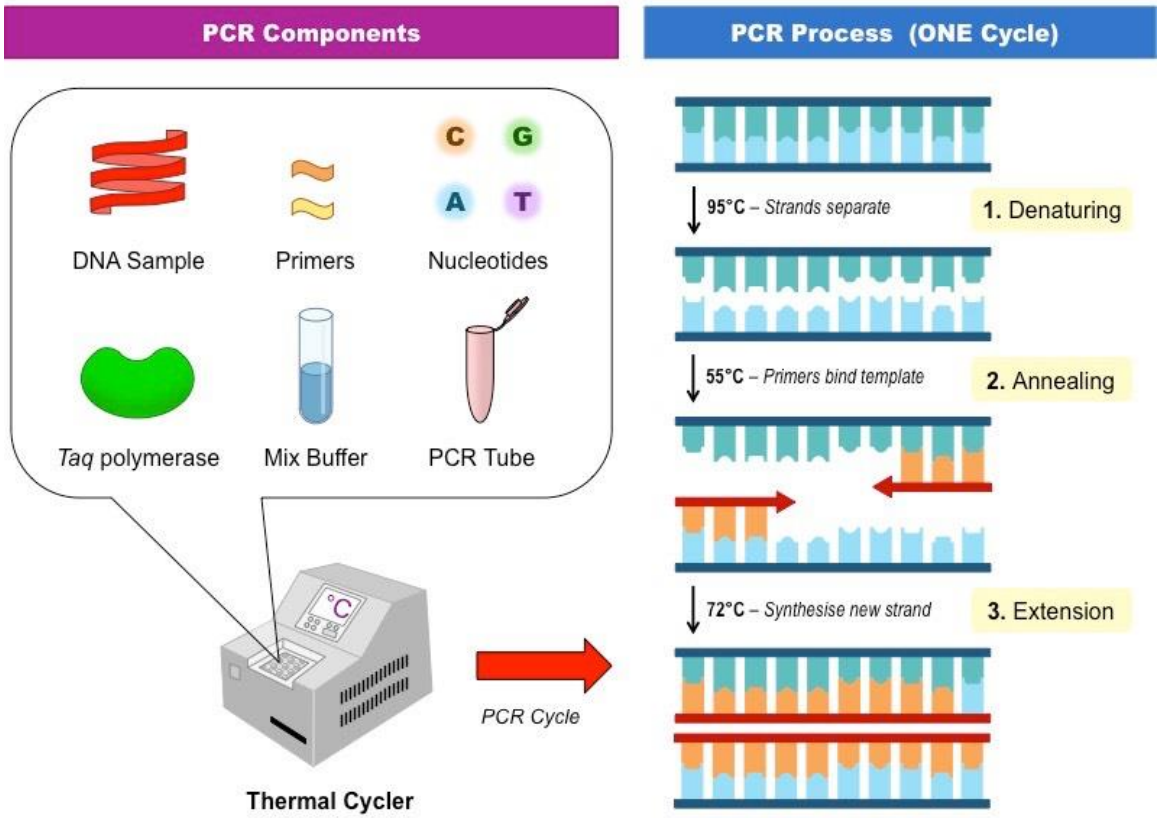

Figure 11: Schematic representation of traditional PCR method.[49]

Several variations of the standard PCR have been developed by researchers to increase the sensitivity of this method. Real-time PCR (RT PCR) and multiplex PCR are the most common methods. Real-time PCR uses fluorescence probe to detect the targeted gene in the PCR cycle in real time not after its end. RT PCR method increases the sensitivity and speed of the PCR-based detection method. Multiplex PCR involves multiple primers for the detection of multiple targeted DNA sequences in one PCR cycle.[50-51]

2.5 Emerging Methods

2.5.1 Surface Plasmon Resonance (SPR) based detection

The SPR-based sensors are a well-established unique platform which is used for analyte detection. In SPR detection of an analyte, the bioreceptor or ligand is primarily immobilized on a gold SPR sensor chip and then the analyte passes throughout the ligand via a microfluidic channel. This will give real-time monitoring of the analyte-ligand interaction, and it can determine thermodynamic parameters such as affinity constant k_A as well as kinetic parameters including k_a and k_d.[52-53]

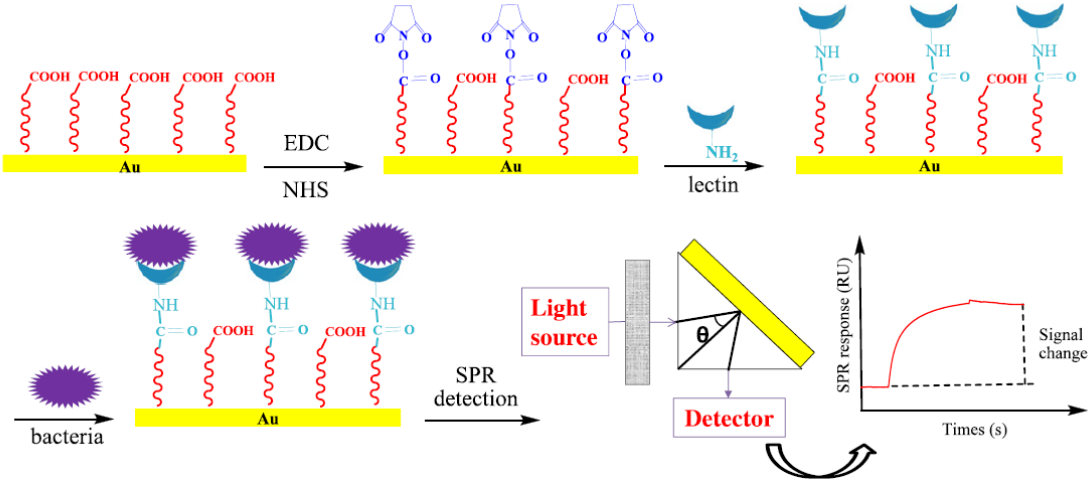

Figure 12: Scheme of the lectin-based surface plasmon resonance biosensor for *E. coli* O157:H7 detection.[53]

Ying et al. developed the SPR-based sensor for the detection of *E. coli* O157:H7 using five types of lectins. The study shows the detection limit of 3 x 10^3 cfu mL^{-1} of *E. coli* O157:H7 by using lectin obtained from Triticum vulgaris as a ligand (**Figure 12**). Moreover, this lectin based SPR sensor is successfully able to detect *E. coli* O157:H7 in a food sample.[53]

2.5.2 Magneto-fluorescent nanosensor

Santra et al. developed a multimodal magneto fluorescent nanosensor (MFnS) for the detection of bacterial contamination using two modalities magnetic and optical. Iron oxide nanoparticles (IONP) are conjugated with monoclonal antibodies specific to *E. coli* O157:H7. When the nanosensors are mixed with bacterial suspension, they will bind with the bacteria's outer membrane due to specific interaction between bacterial epitopes and antibodies. As a result of these clusters, interaction between these nanosensors and water protons is hindered and the resultant magnetic relaxation time (ΔT2) increases. In the presence of low CFUS, ΔT2 is higher because of the large degree of magnetic nanosensor clustering; however, in the presence of high CFU numbers, ΔT2 is smaller because the nanosensors are dispersed in the sample with bacteria. The fluorescence modality uses 1, 1'-Dioctadecyl-3, 3, 3', 3'-Tetramethylindocarbocyanine Perchlorate (DiI) dye encapsulated in a polyacrylic acid coating of IONP. The fluorescence modality is useful in the detection of high numbers of CFUs. In the presence of low CFU numbers, because of centrifugation process after incubation with target bacteria, the unbound MFnS will be removed from the suspension and the low number of nanosensor bound to low CFUs gives low fluorescence emission. The presence of high CFU numbers leads to large numbers of nanosensors in the sample after centrifugation and produces higher emission intensity. Santra et al. have successfully developed the nanosensors able to detect the *E. coli* O157:H7 at concentrations as low as 1 CFU with magnetic modality and higher CFUs with fluorescence modality (**Figure 13**).[54]

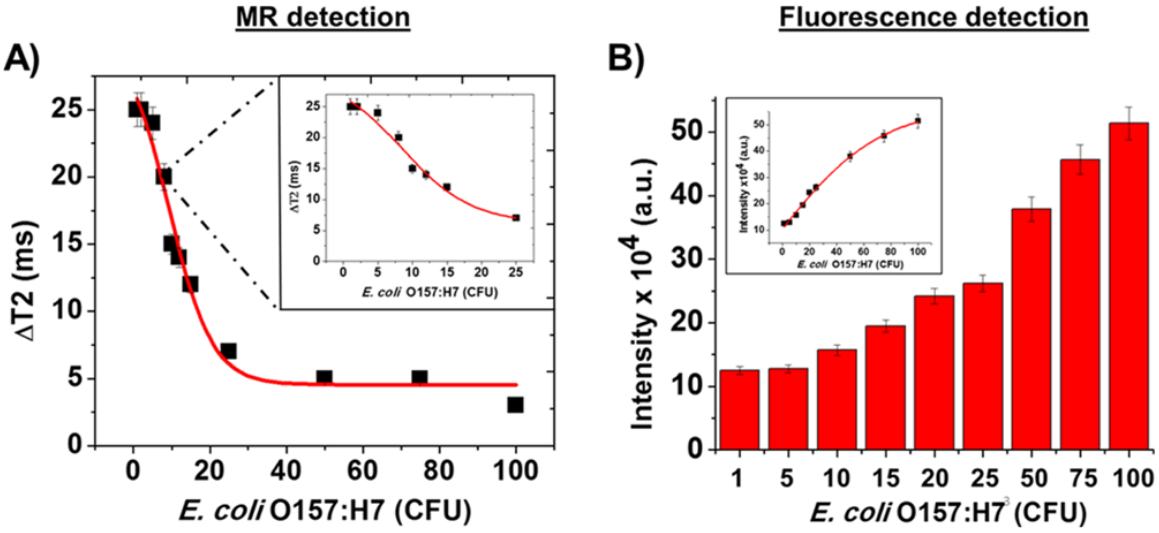

Figure 13: (A) Detection of *E. coli* O157:H7 in PBS solvent using magnetic property (changes in magnetic relaxation ΔT2) of MFnS (inset: CFU ranges from 1 to 20). (B) Fluorescence emission data collected from the same contaminated sample (inset: linearity plot).[54]

2.5.3 Colorimetric Detection of *E. coli* using Gold Nanoparticles

Gupta et.al. developed a colorimetric detection method for the detection of *E. coli* based on gold nanoparticle (AuNP) aggregation. They developed a single stranded DNA aptamer specific to *E. coli.* A coating of graphene oxide (GO) on AuNPs increased the loading capacity of the aptamer. Using 1-ethyl-3-(3-(dimethylamino) propylcarbodimide hydrochloride (EDC), *N*-hydroxysuccinimide (NHS) chemistry aptamer was fabricated on AuNP-GO (GO coated AuNPs). In the presence of *E. coli* cells, the aptamer attaches to the bacteria's cell surface causes the aggregation of AuNPs (**Figure 14)**. Visually, a colorimetric shift from red to blue can be seen, as well as a red shift in the distinctive surface plasmonic peak of AuNPs. In the absence of *E. coli* cells, the nanoparticles stay dispersed, no aggregation is detected, and it remains in red color.

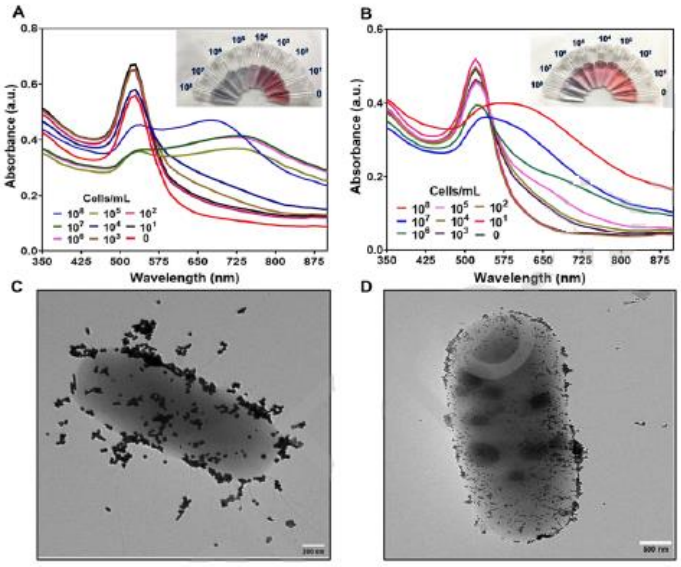

Figure 14: UV-Vis spectrum of (A) Aptamer conjugated GO-AuNPs with increasing concentrations of *E. coli* cells (inset: colorimetric change) and (B) Aptamer conjugated citrate AUNPs with *E. coli* cells (inset: colorimetric change). TEM image of (C) *E. coli* cells with aptamer conjugated GO-AuNPs, and (D) Aptamer conjugated citrate AuNPs with *E. coli* cells.[55]

The limit of detection for this assay was 10^2 cells mL^{-1} for AuNP-GO and 10^3 cells mL^{-1} without coating of GO on AuNP. This detection method was observed to be suitable for use in glass capillaries, which can be useful for producing point-of-care detection devices.[55]

Conclusion

The occurrence and significance of foodborne infections is increasing worldwide. The development of the food industry at international scale, variations in food manufacturing systems, and the population of humans and their waste has led to frequent infections. As previously discussed, *E. coli* O157:H7 is a major foodborne pathogen. The frequency of infectious outbreaks demonstrates the need for an efficient and reliable method for the detection of this pathogen. Culture based methods are simple and inexpensive, but these methods are time consuming and can require up to a week to obtain results. These methods are not rapid enough or reliable enough for early-stage detection of pathogens. PCR is advantageous over culture-based methods, but the ability to amplify the DNA of dead cells is a major drawback for detection of live pathogens. The method introduced in this thesis can strategically replace conventional methods and can reduce the time and cost for the detection of pathogens in food samples.

Chapter II

Results and Discussion

1. Introduction

Foodborne outbreaks and diseases are on the rise in the United States.[1] Foodborne illnesses pose a significant health and economic burden, with the Centers for Disease Control (CDC) estimating 48 million illnesses, 128,000 hospitalizations, and 3,000 deaths each year.[2] Consumption of contaminated food or water is the most common mode of transmission[3], and *Escherichia coli* (*E. coli*) plays a key role in infection, with some *E. coli* strains linked to foodborne illnesses in international scale outbreaks.[4-5] Shiga toxin-producing *E. coli* (STEC) serotype O157:H7, the most lethal strain, first emerged as a significant public health risk in the 1980s.[6] Despite strict oversight and regulations in most countries, produce-associated outbreaks are on the rise, with recent outbreaks traced to leafy salad greens around the world.[7-9] The CDC and the Food and Drug Administration have yet to identify the source(s) of two *E. coli* O157:H7 infections, both of which were found to be caused by STEC strains. This year, the United States dealt with three highly publicized multistate outbreaks.[10] STEC was recently identified as the cause of 1 million illnesses, 100 deaths, and 13,000 disability-adjusted life years by the World Health Organization (WHO).[11] Because STEC has a very low infection dose of only 10-100 organisms and spreads through person-to-person contact, rapid spread is not surprising.[8] STEC verotoxins are known to be virulent to humans, causing gastrointestinal disease all over the world, including life-threatening hemolytic-uremic syndrome (HUS), bloody diarrhea, and hemorrhagic colitis.[12-15] This is especially concerning given that the healthcare industry is dealing with multidrug-resistant bacteria, including drug-resistant strains of *E. coli* that are transmittable to humans via direct and indirect contact with food and water.[16] This emphasizes the significance of rapid, accurate detection in identifying pathogens and reducing contamination and infection caused by consumption of contaminated food or drinking sources.

New methods for disease detection have appeared in recent decades. Iron oxide nanoparticles (IONPs) were considered to be static until the intrinsic peroxidase-like properties of Fe_3O_4 were developed in 2007, launching a new field of research that combines nanotechnology with enzyme biocatalytic activity.[31] Enzymes have long been researched and used because of their strong catalytic activity and selectivity, including in consumer, commercial, and therapeutic applications.[17-25] Enzymes have become indispensable in agrifood detection over the last few decades, with a growing role in food safety issues due to their sensitivity and selectivity in detecting small molecules, ions, proteins, and both biological and chemical contaminants.[25]

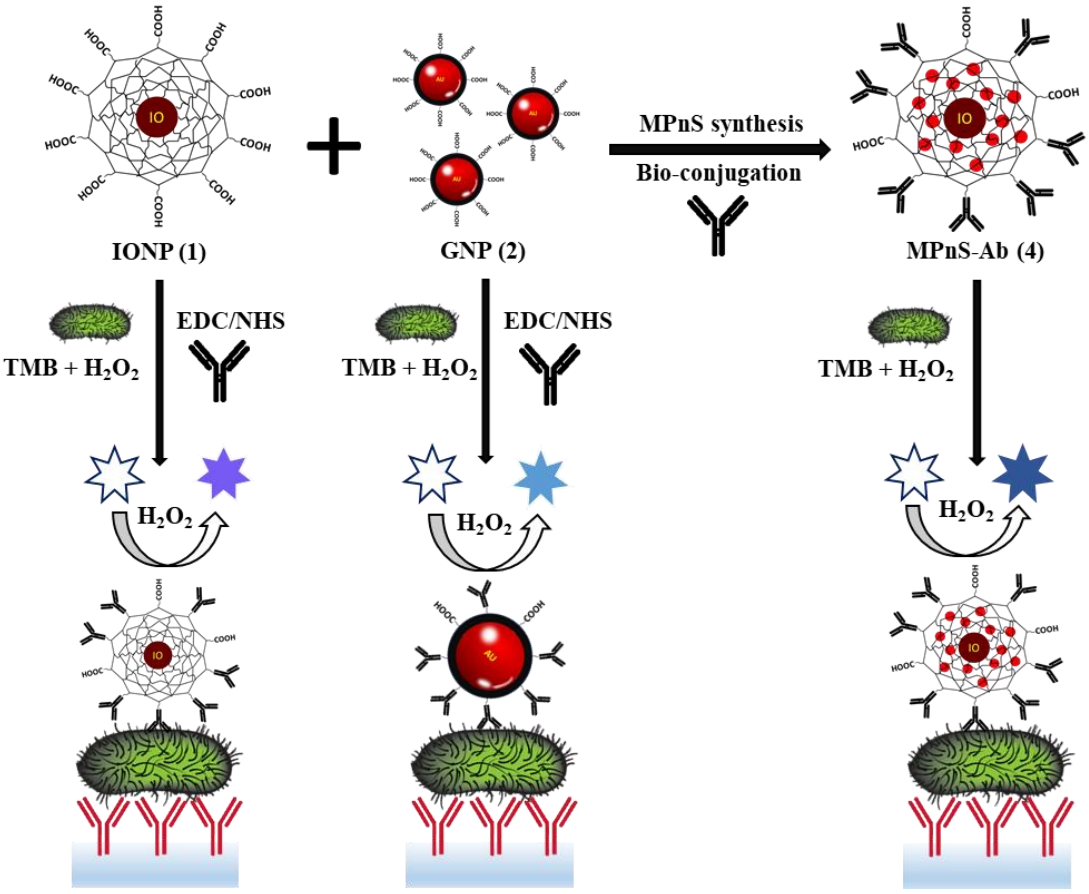

Figure 15. Schematic illustration of nanozyme-mediated ELISA. Synthesis of the magneto-plasmonic nanosensor (MPnS) and it's working principle for detection of *E. coli O157:H7*.

However, environmental limitations have restricted improvement and usage of natural enzymes.[26-27] The disadvantages of these enzymes include expensive preparation and purification costs, instability, rapid denaturation, and recycling and reuse difficulties.[28-30] Since the 1950s, researchers

have been pursuing artificial enzymes as low-cost and reliable solutions to overcome these limitations.[31] This has led to the discovery of materials with comparable structure and function, such as fullerenes, cyclodextrins, polymers, and dendrimers-based enzymes.[32-38] However, concerns about biocompatibility and catalytical efficiently have hindered success. Nanozymes, nanomaterial-based artificial enzymes, are the next generation of artificial enzymes. Significant research in this field has ushered in a new age of enzyme-mimetic investigation, resulting in a new concept called nanozymology, which combines nanotechnology with biology.[39] There are currently approximately 300 different kinds of nanomaterials having inherent enzymatic capabilities.[40] Nanozymes, which have the functional properties of enzyme mimics, catalyze the same biocatalytic reactions as natural enzymes even with extreme pH and temperature.[41] As a result, nanozymes are becoming more widely used in the detection of ions, proteins, small compounds, and biological pollutants in agrifood.[42] Nanozymes have also fueled many of biological breakthroughs, including immunoassays, biosensors, and antibiofilm and antibacterial agents.[43-44] Peroxidase, oxidase, catalase, and superoxide dismutase enzymes have all been reported to exhibit catalytic activity in nanomaterials.[45-50] Nanozymes are suitable for pathogen detection because they can attach to antibodies and detect analytes of interest. They have the same oxidation function as horse radish peroxidase (HRP), which is also the foundation for the well-known ELISA assay.[51] They also feature multi-enzyme mimic activity, improved stability, and durability for reduced manufacturing costs, are simple to mass-produce, have adjustable activity, and a wide surface area for multi-functionalization.[30,52-55]

2. Results and Discussion

This study proposes a novel strategy to synthesize a magneto-plasmonic nanosensor (MPnS) composed of IONP and GNP, with unique peroxidase activity against the TMB peroxidase substrate model (**Figure 15**) and rapid detection of *E. coli* O157:H7, a pathogen known to be infectious at low CFU counts. The MPnS synthesis involves two steps: (1) synthesis of polyacrylic acid (PAA) coated IONPs,[56] and (2) *in situ* GNP synthesis using Turkevich method encapsulation in PAA coating of IONP.[57] The protocol for synthesis of IONP-PAA was used as previously reported.[56] Gold salt ($HAuCl_4$) boiled along with prepared IONPs followed by the addition of sodium citrate which results in the reduction of gold (III) to gold (0) which is concurrently entrapped within the PAA coating of IONPs. The emergence of ruby red color (max = 522 nm) indicates completion of reduction, which is also utilized to assess the endpoint for MPnS synthesis. To optimize the synthesis of MPnS, we also conducted preliminary experiments to synthesize gold

nanoparticles with different ratios of $HAuCl_4$ and citrate according to the reported "Turkevich" procedure.[57] Free GNPs were removed through magnetic column in order to purify the MPnS. MPnS expresses carboxylic group (COOH) on the surface which can be functionalized with the specific antibody for the target bacteria.[58] We hypothesized that, the successful MPnS synthesis combines the IONPs with GNPs which results in synergistic interactions improving the catalytic properties of both nanoparticles individual intrinsic enzymatic activity. The peroxidase-like activity of the produced enzyme-mimetics was employed in a colorimetric test, which is reliant on the oxidation of the peroxidase substrate TMB by H_2O_2, which results in a color shift from clear to blue. The greater the enzymatic efficiency, the more intense the color. The antibody conjugation was required for the creation of a "sandwich ELISA" comprising of MPnS coupled to detection antibody and TMB, which will undergo a redox reaction in the presence of the target pathogen, resulting in a visible color change. This is based on the fundamental idea of "sandwich ELISA," which is one of the most well-known and successful methods for detecting *E. coli* O157:H7. Furthermore, it is grounded in the basic premise that unbound antigens are eliminated in subsequent washes and that no color change occurs until the intended antibody-antigen interaction occurs. As seen in **Figure 15**, the most dramatic color shift, a deeper blue, was observed with functioning MPnS-Ab. As a result, we decided to test our hypothesis that MPnS might be utilized as a fast and highly specific colorimetric method for pathogen identification.

3. Characterization Studies of MPnS and MPnS Conjugates:

To confirm the successful synthesis of MPnS, characterization experiments were conducted using dynamic light scattering (DLS), T2 relaxation, UV-Vis analysis, TEM and EDS. DLS experiments were carried out using Zetasizer Nano-ZS90. DLS experiments were performed to measure the average size and zeta of MPnS before and after conjugation with antibody. The average hydrodynamic radius of MPnS found to 72 nm and after conjugation with anti- *E. coli* antibody it increases to 78 nm **(Figure 16A)**. The zeta potential also showed effective conjugation, with a shift in negative surface charge from –28 to –11 mV in the before and after conjugation, respectively **(Figure 16B)**. MPnS is a nanocomposite of IONP and GNP, Citrate stabilized GNP are situated in the cargo space of PAA coating of IONPs. TEM analysis shows the small dots in PAA coating of

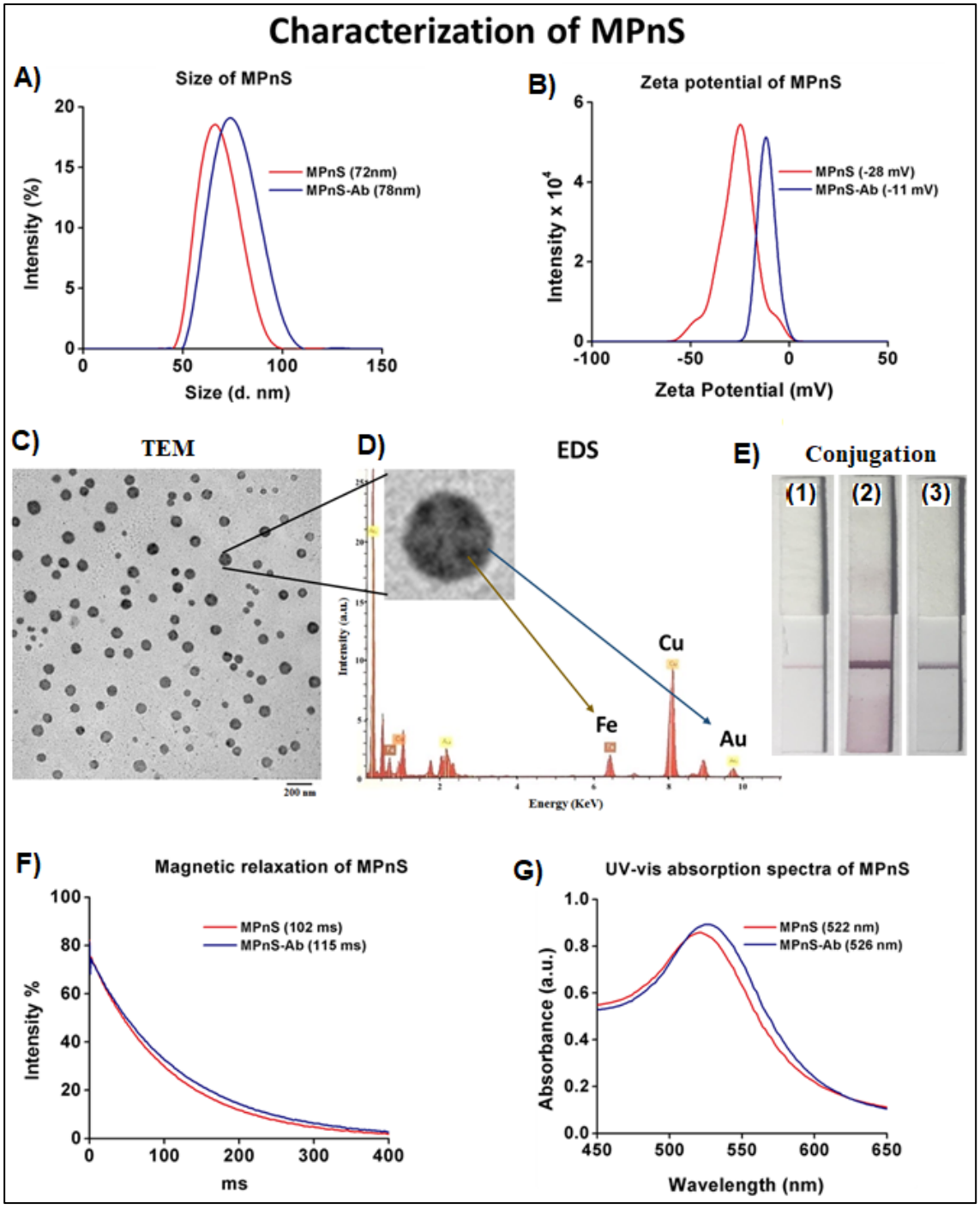

Figure 16. Characterization of MPnS and antibody conjugated MPnS: (A) Hydrodynamic radii of MPnS before and after conjugation and (B) zeta potential of MPnS and MPnS-Ab. (C) Transmission Electron Microscopy (TEM), Scale Bar: 200 nm and (D) energy-dispersive X-ray spectroscopy (EDS). (E) Images of the conjugation half strips, confirming for the successful antibody conjugation 1) Positive control, 2) on GNPs and 3) on MPnS. (F) T2 magnetic relaxation

of MPnS and MPnS-Ab, and (G) UV-Vis absorption spectra of MPnS and MPnS-Ab, further confirming successful conjugation.

IONP, which is GNP. Elemental analysis was further determined by EDS **(Figure 16C-2D)**. Moreover, the Conjugation Check & Go kit from Abcam was used for the further confirmation of conjugation. Development of a visible red line on the protein A/G strip indicates the antibodies conjugated on the surface of MPnS. **(3, Figure 16E)**. In addition, as previously described in the literature, we employed the T2 relaxation diagnostic method. In summary, binding of target analytes causes water molecules to be displaced, resulting in detectable changes in the spin-spin magnetic relaxation time (ΔT2). This was seen with the MPnS measured at 102 ms and the MPnS-Ab increased to 115 ms **(Figure 16F)**.

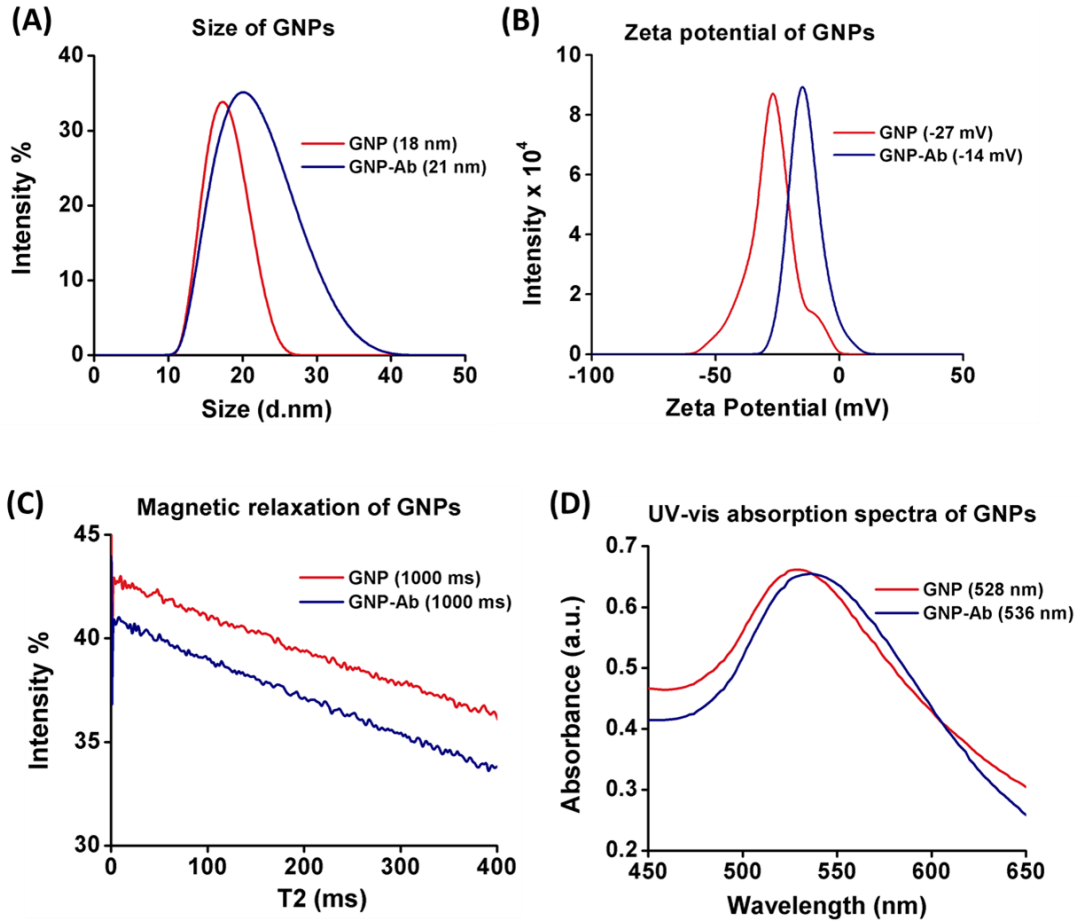

Figure 17. Characterization of GNP and antibody conjugated GNP: (A) Hydrodynamic radius of GNP before and after conjugation, (B) Zeta potential of GNP and GNP-Ab. (C) T2 –relaxation of GNP and GNP-Ab (D) UV-vis absorption spectra of GNP and GNP-Ab further confirming successful conjugation.

The final verification method used to evaluate successful conjugation of Abs, was with optical absorption by exploiting the UV-Vis properties of gold (SPR). UV-Vis absorption spectra demonstrated the conjugation reaction occurred with the unbound MPnS measured at 522 nm compared to MPnS-Ab at 526 nm (**Figure 16G**). The red shift in SPR indicated for the successful conjugation.

4. Characterization Studies of GNPs and IONPs:

Similar experiments were performed for the confirmation of successful synthesis and conjugation for both GNPs and IONPs. The average hydrodynamic size and zeta potential for the GNPs before

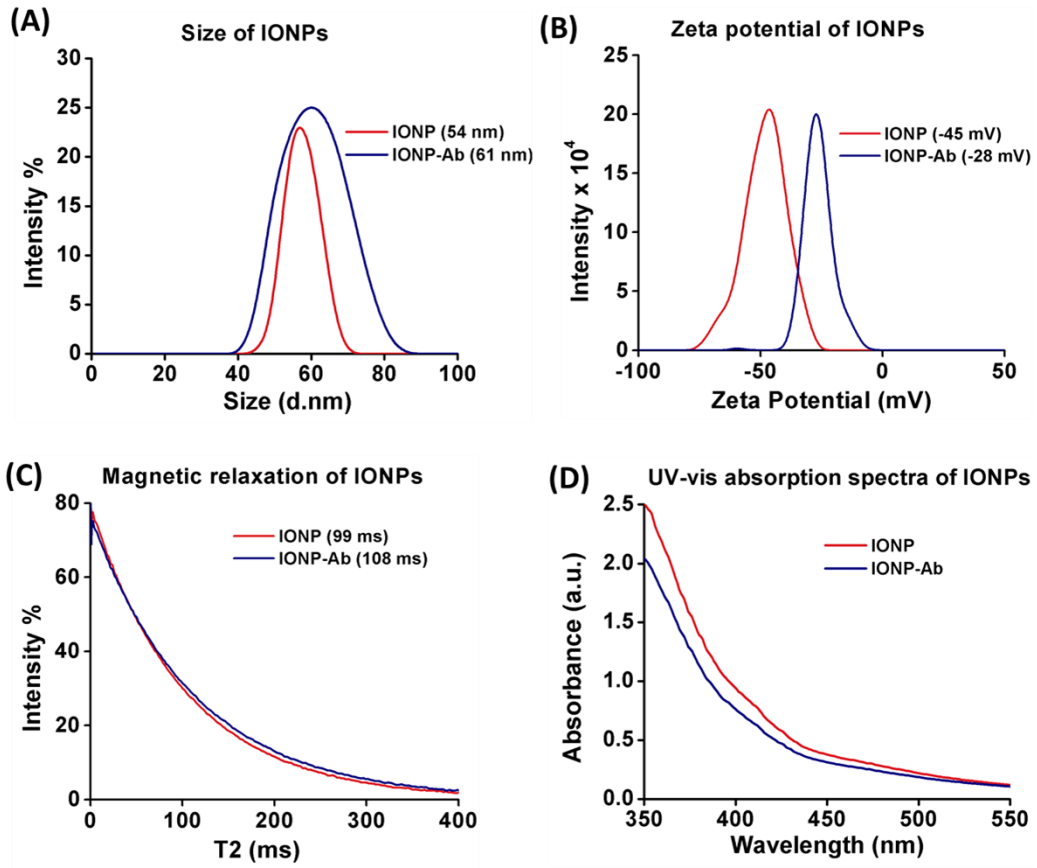

Figure 18. Characterization of IONP and antibody conjugated IONP: **(A)** Hydrodynamic radii of IONP before and after conjugation **(B)** Zeta potential of IONP and IONP-Ab. **(C)** T2 –relaxation of IONP and IONP-Ab **(D)** UV-vis absorption spectra of IONP and IONP-Ab further confirming successful conjugation.

and after conjugation were 18 nm and 21 nm and -14 mV and -27 mV, respectively **(Figure 17A-3B)**. We also assessed conjugation using our T2 relaxation approach and UV-Vis absorption spectra measurements for conjugation of *E. coli* antigen specific Abs to GNPs. Higher T2 relaxation values showed that GNPs had weak magnetic characteristics **(Figure 17C)**; nevertheless, effective conjugation was indicated by red SPR shifts in UV-Vis absorption spectra, which changed from 528 nm to 536 nm **(Figure 17D)**. Similarly, a discernible line on the protein A/G test strip demonstrated that the antibody conjugation was effective **(2, Figure 16E)**.

Similar characterization experiments, size measurement, zeta potential, T2 relaxation and UV-Vis were performed for the verification of successful synthesis and conjugation of IONPs. After conjugation, the size increases from 54 to 61 nm (Figure 4A) and zeta potential deceases from -45 mV to -28 mV **(Figure 18B)**. T2 relaxation values shows the magnetic property of IONPs; changes in ΔT2 relaxation from 99 ms to 108 ms for unconjugated and conjugated IONPs indicate the effective conjugation of antibodies on the surface. The above results showed the successful conjugation of MPnS, GNPs and IONPs. Moreover, aqueous stability was carried out by measuring the overall hydrodynamic diameter for MPnS, GNPs and IONPs before and after conjugation at room temperature. (**Figure 19** and **Table 1**) These data further demonstrated the prolonged stability of the synthesized functional nanoparticles, which is important for point-of-care applications.

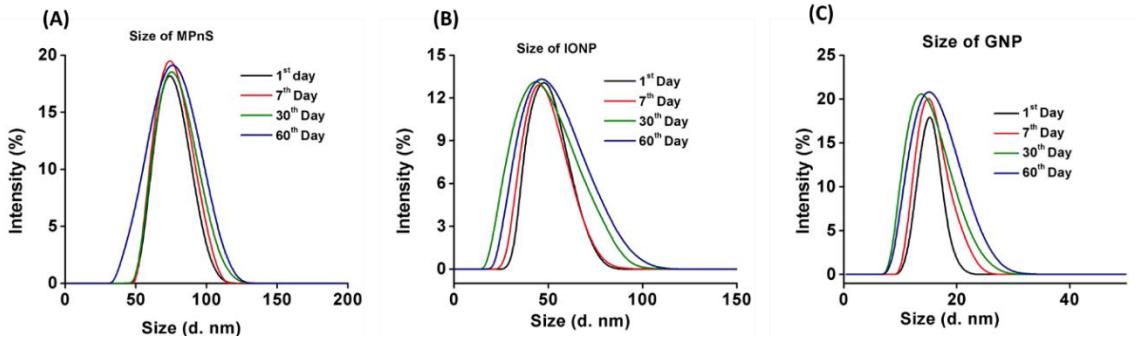

Figure 19: Size of nanoparticles over a period of two months (A) MPnS, (B) IONP, and (C) GNP.

Nanoparticle	1st Day	7th Day	30th Day	60th Day
MPnS	72 ± 2 nm	72 ± 2 nm	74 ± 3 nm	82 ± 5 nm
MPnS-mAb	77 ± 2 nm	76 ± 3 nm	78 ± 5 nm	88 ± 6 nm
IONP	54 ± 2 nm	53 ± 3 nm	56 ± 2 nm	59 ± 5 nm
IONP-mAb	59 ± 2 nm	60 ± 2 nm	62 ± 4 nm	66 ± 6 nm
GNP	16 ± 2 nm	16 ± 2 nm	15 ± 3 nm	18 ± 3 nm
GNP-mAb	21 ± 2 nm	20 ± 2 nm	22 ± 4 nm	27 ± 5 nm

Table 1. Stability of nanoparticles over 2 months of period in 1X PBS (pH 7.4). IONP stored at room temperature, GNP and MPnS stored at 4° C.

5. Optimization Studies

Certain factors must be considered when assaying natural enzymes with a standardization of parameters including temperature, pH, and substrates being ideal. This is complicated, and especially, when more than one enzyme is used due to the varying intrinsic properties of the enzymes themselves. The enzyme process itself generates pH changes and can influence enzymatic activity. We investigated critical parameters for individual nanozymes in this study, and the composite of the IONPs and GNPs provides more insight into the synergistic effects when employed together in MPnS. We studied the impact of altering the following variables on the catalytic activity of our nanozymes: H_2O_2, pH, temperature, and size **(Figure 20)**. We used horseradish peroxidase (HRP) as control, this natural enzyme has been used and studied significantly in a range of biochemical applications. Testing these characteristics also verified the nanozyme's improved stability and endurance of our MPnS, as well as our prediction that combining the IONPs and GNPs would result in increased enzymatic capabilities. The natural enzyme HRP shows high activity at about 0.1 M H_2O_2 concentration and, as predicted, denatures quickly, revealing a relatively limited window for catalytic activity. While IONPs and GNPs have longer and more consistent catalytic activity than HRP, MPnS begins to demonstrate steady enzymatic activity about 0.5 M and continues with a modest increase in activity around 1.0 M **(Figure 20A)**. For the optimization of pH, again HRP peaks in catalytic activity nearly pH 2.5, but dramatically reduced from minimum to no activity at pH 7. The GNPs and IONPs shows maximum activity at about pH 5 following a parabolic curve; MPnS exhibits the most stability with reasonably high activity from pH 2.5 to pH 6.0 with enzymatic activity present, as observed with the IONPs,

and until the test completed at pH 9.0 **(Figure 20B)**. This is noteworthy since natural enzymes are very sensitive to pH, as proven by HRP, and suggests that MPnS might be dependable under harsher environments. Both nanozymes and enzymes were less temperature sensitive, however the MPnS and GNP nanozymes surpassed both the IONPs and HRP and remained gradually active even though temperatures varying from 20 to 60 °C **(Figure 20C)**. Particularly noteworthy are concerns about pH and temperature being regarded as independent factors rather than examining the combined effect when using more than one enzyme [59], which these investigations may assist to clarify. We find it intriguing that the IONPs show better resilience to changing pH than the GNPs nanozyme, which is then reversed in temperature assessments of enzymatic activity. When merged, the resulting MPnS nanozymes outperform the individual nanozyme.

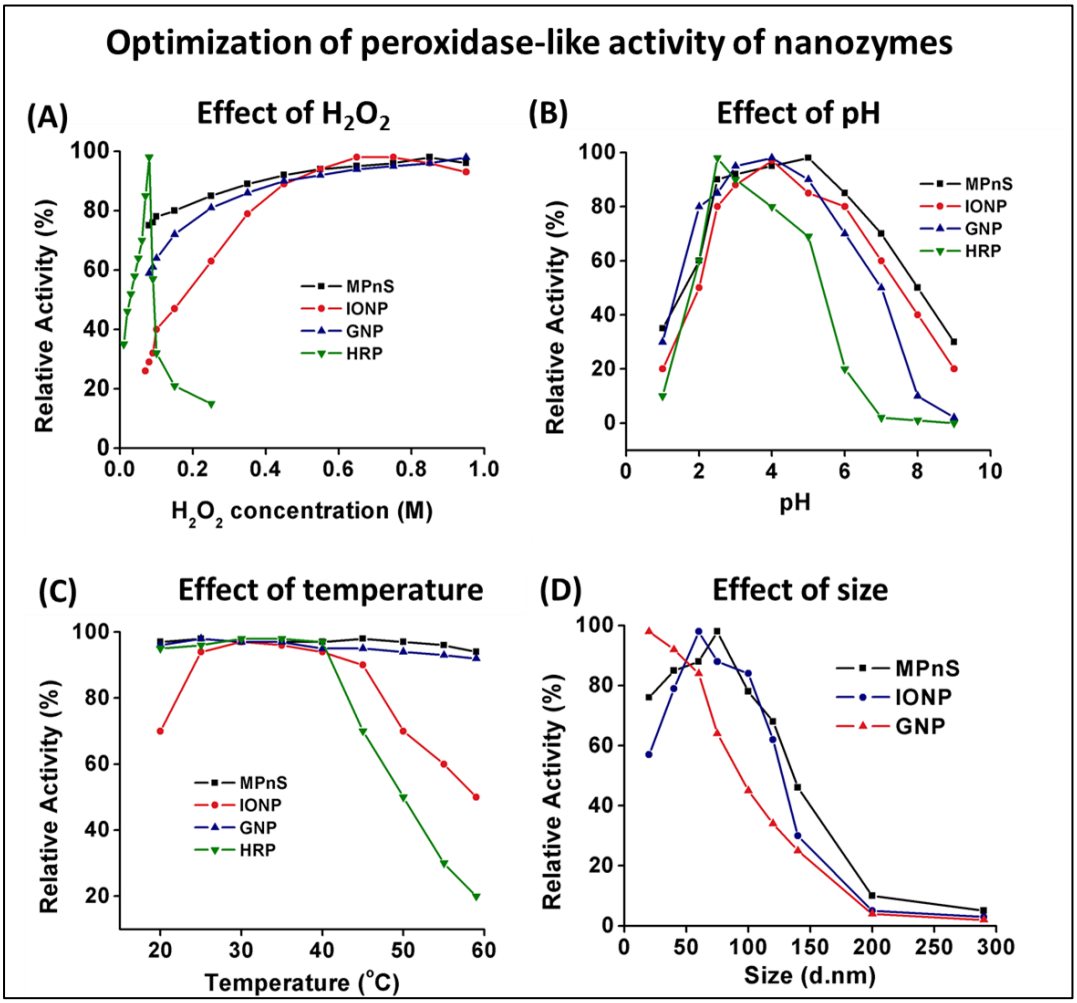

Figure 20: Optimization of peroxidase-like activity of nanozymes and natural enzyme with (A) varied H_2O_2, (B) pH, (C) temperature and (D) hydrodynamic diameter.

Enzymatic activity is largely dependent on optimal conditions. These investigations show that the length of enzymatic activity observed in the MPnS under different circumstances demonstrates the necessary stability required for identifying infections in a wide range of environments, as found in the agrifood field/industry. We studied the effect of nanozyme size on catalytic activity for the further improvement of detection sensitivity **(Figure 20D)**. we analyzed different sizes of the nanozyme and its optimum activity. The size of the GNP appears to be directly related to activity, with smaller being more active and bigger being less active, the MPnS and IONP both indicated optimum size to be approximately 75 nm.

6. Peroxidase-Like Catalytic Activity of Nanozymes

With a growing number of nanozyme applications and the fact that their catalytic activity is dependent on physiochemical characteristics such as shape, size, and composition, and characterization of our MPnS was critical to this project. Our technique is based on Jiang et al.'s work, which demonstrated a consistent and dependable catalytic standard for measuring and defining nanozyme catalytic activity using Michaelis-Menten kinetics **(Figure 21).** H_2O_2 concentrations were held constant while 3,3,5,5-tetramethylbenzidine (TMB) was increased to find V_{max}, the maximum reaction rate defined by substrate concentration saturation for HRP, GNPs, IONPs, and MPnS. As expected, HRP demonstrated the maximum V_{max} at 8.7 x 10^{-8} M/s **(Figure 21A)**, Michaelis-Menten kinetics showed each nanozyme surpassed the HRP's catalytic activity (k_{cat}). K_m shows how rapidly the reaction accelerates with increasing substrate concentration, indicating the substrate affinity. The stronger the affinity, the lower the K_m. Our studies show that GNPs has the highest affinity, with a K_m value of 96 M. Each synthesized nanozyme exhibited much higher affinity than HRP, which had the greatest K_m at 243 M **(Table 2)**. However, when evaluating the catalytic constant, k_{cat}, representing the number of substrate molecules each enzyme converted into product, IONPs and GNPs showed a 10-fold higher k_{cat} values than HRP. Additionally, MPnS exhibited the highest k_{cat} value, with a 100-fold difference at 5.9 x 10^5 in comparison with HRP at 4.3 x 10^3. We hypothesized that a customized "sandwich ELISA" employing the MPnS might result in a viable and robust colorimetric pathogen detection method because of this enormous increase in activity.

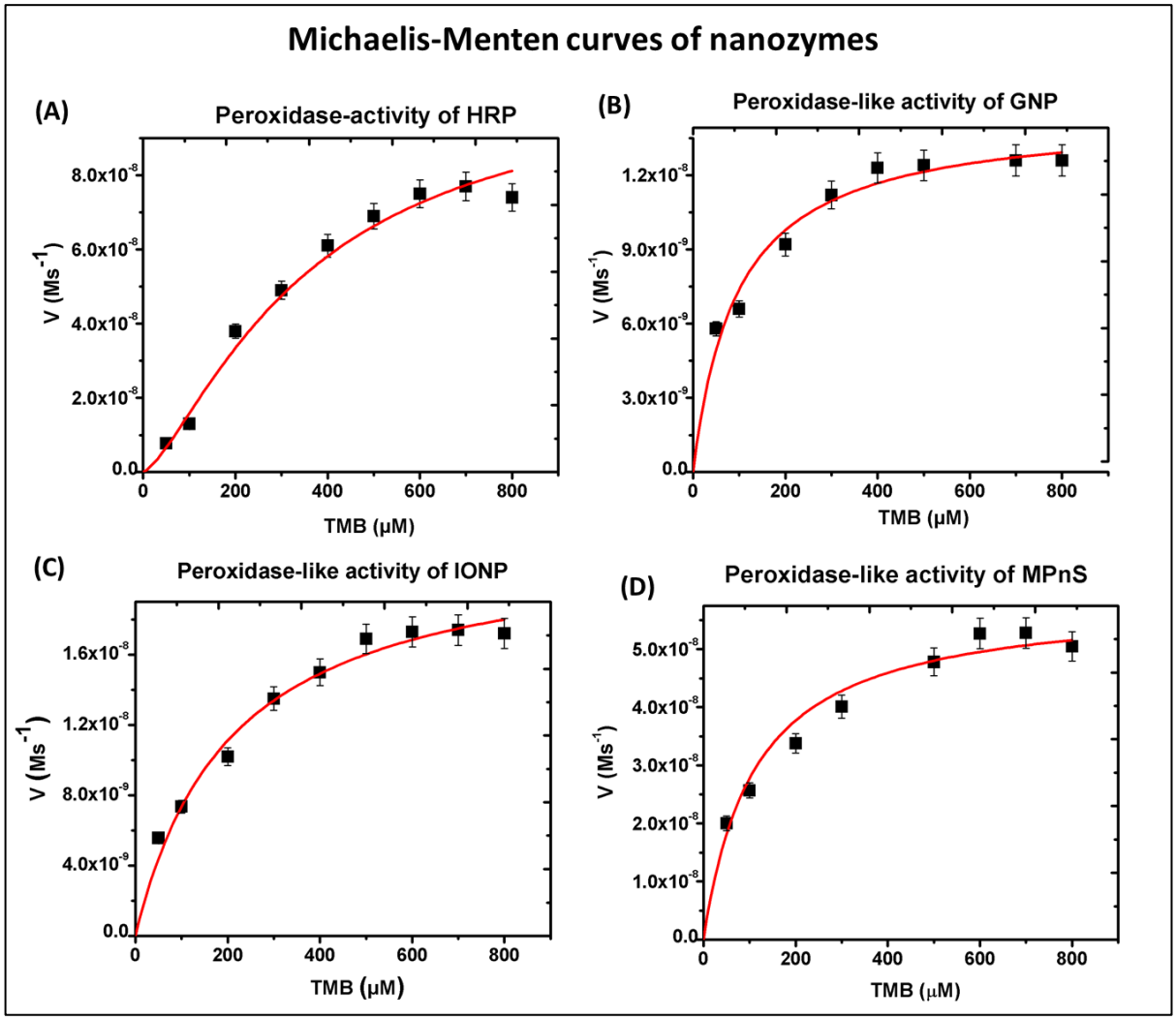

Figure 21: Kinetic parameters of nanozymes and natural enzyme HRP exhibiting peroxidase activity: Steady state kinetic analysis using Michaelis-Menten Model of (A) HRP (B) GNPs (C) IONPs and (D) MPnS by varying TMB concentrations.

Catalyst	K_m (μM)	V_{max} (10^{-8}M/s)	k_{cat} (s)
HRP	243	8.7	4.3×10^3
IONP	208	2.3	2.5×10^4
GNP	96	1.4	2.4×10^4
MPnS	111	5.9	5.9×10^5

Table 2: Kinetic parameters of IONPs, GNPs, MPnS and HRP nanozymes obtained from Michaelis-Menten curves. K_m denotes the Michaelis constant, V_{max} is the maximum velocity, [E] is

total enzyme concentration, k_{cat} is the catalytic constant and is expressed by the formula $k_{cat} = V_{max}/[E]$.

7. Optimization of concentration of detection antibody for stable conjugate assessment

Flocculation studies were carried out to identify the stabilizing concentration of Anti-*E. coli* O157:H7 mAb for conjugation with MPnS. Initially, several MPnS conjugates were produced using mAb. The mAb concentration for conjugation was maintained between 0.5 and 16 µg/mL. Because no aggregation was seen during synthesis, stable and efficient conjugates were produced. Furthermore, the presence of a discernible line on the protein A/G test strip (half-strip) demonstrated that the antibody had been properly conjugated **(Figure 22A)**. When 10% NaCl was given to each of these conjugates, however, alterations in OD_{580} were detected, as shown in **Figure 22B**. The optical density increased with increasing Mab concentration, from 0.5-2 µg/mL, suggesting flocculation. Furthermore, when 10% NaCl was added to these conjugates, they became blue, indicating that the conjugates were unstable. However, above 2 µg/mL, there was a significant reduction in optical density, which eventually reached a plateau. Furthermore, the color of these preparations was brilliant red, indicating effective and stable conjugate synthesis **(Figure 22B inset)**. The MPnS conjugate produced with 8 µg/mL Mab concentration was chosen for the ELISA tests based on the flocculation curve.

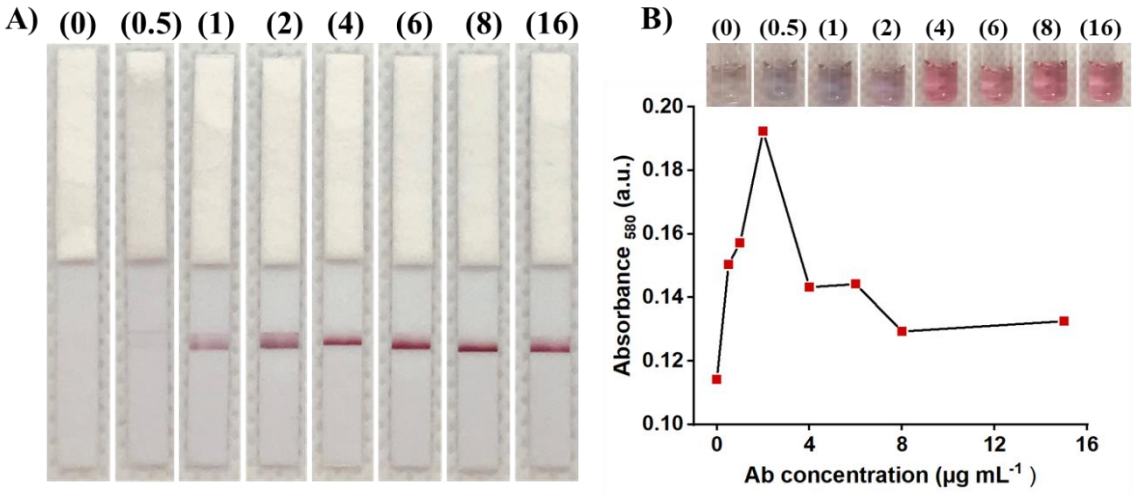

Figure 22: Flocculation curve of MPnS-MAb conjugates at varied MAb concentrations. (A) Protein A/G strips, (B) Absorbance of GNP-Mab conjugated at 580 nm after addition of 10 % NaCl (inset: colorimetric appearance after addition of NaCl).

8. Peroxidase-based Sandwich ELISA for the Detection of *E. coli* O157:H7

We used sandwich ELISA format to demonstrate the superior peroxidase-mimetic activity of GNPs, IONPs, MPnS, and HRP in biosensing applications **(Figure 23)**. The absorbance of TMB was measured at 652 nm, the highest absorbance of oxidized TMB, to illustrate the sensitivity of

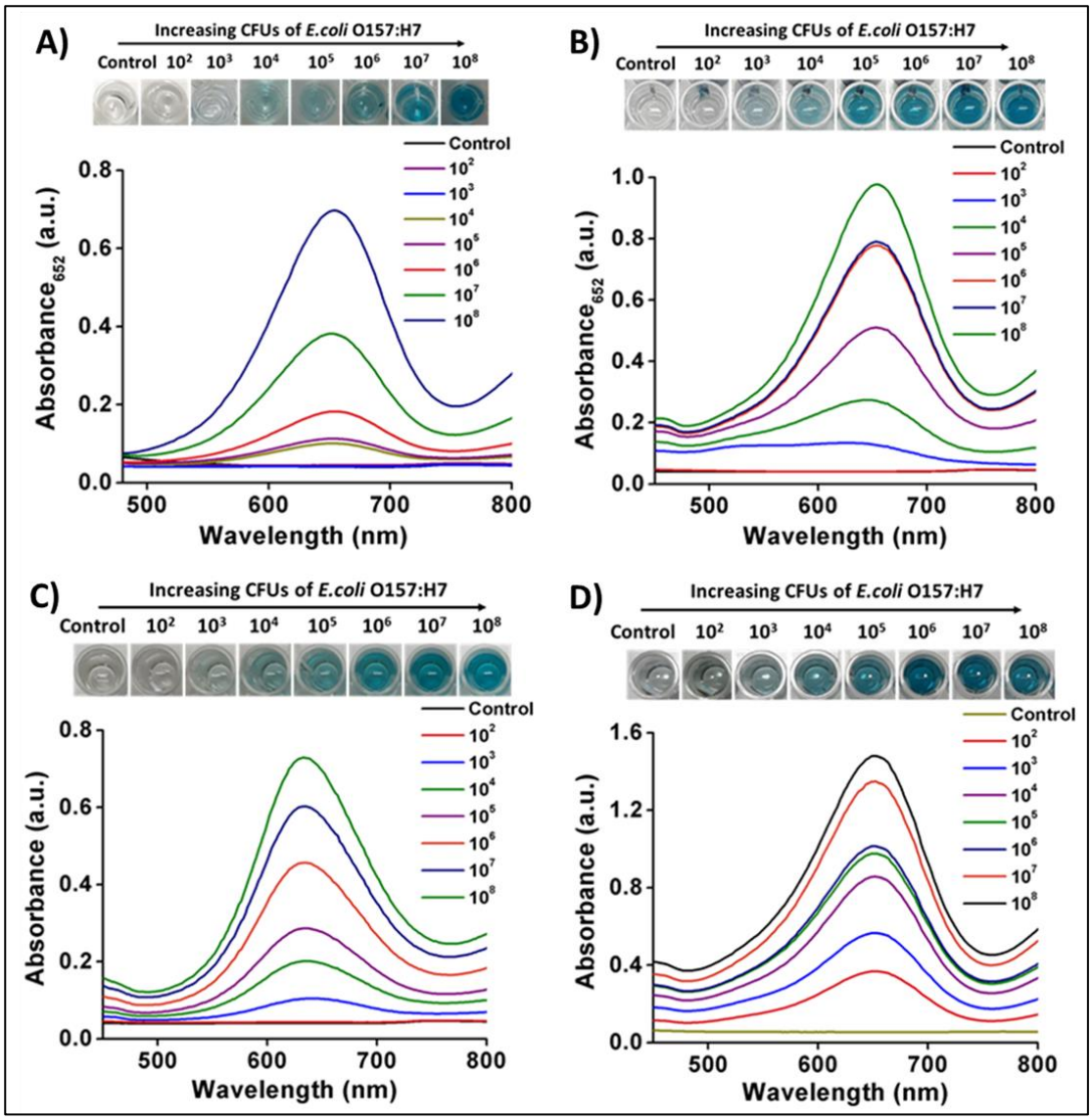

Figure 23: Colorimetric and SPR detections of different CFUs of *E.coli O157:H7* spiked in 1X PBS using A) HRP, B) GNPs, C) IONPs, D) MPnS in conventional "sandwich ELISA" format. The absorbance of TMB at 652 nm was plotted as a function of different CFUs of bacteria.

natural and manufactured enzymes to *E. coli* O157:H7 colony forming units (CFUs). The rate of oxidation in the "sandwich ELISA" coupling contact with target bacteria was measured using a colorimetric test and absorbance measurements. Color changes were not visible with HRP until CFU concentrations reached 10^4, and then color intensity steadily altered as concentration increased **(Figure 23A)**. Notably, at concentrations of 10^3, the GNPs and IONPs showed visible color variations and an increase in absorbance **(Figure 23B-C)**. MPnS, on the other hand, demonstrated a noticeable change in color and absorbance at a concentration of 10^2, showing a 100-fold improvement in detection sensitivity as anticipated by the kinetic studies **(Figure 23D)**. When comparing HRP to all three nanozymes, there was also a significant change in color intensity as bacterial densities grew. Furthermore, **Figure 24** shows that our MPnS may be utilized as a very sensitive detection assay for *E. coli* O157:H7 by visually comparing the detection sensitivities of HRP with nanozymes and providing side-by-side absorbance differences.

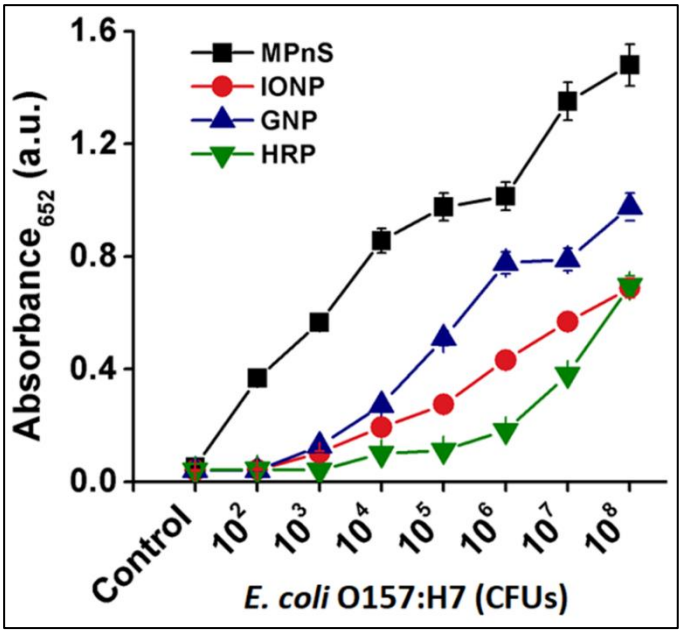

Figure 24: Plot comparing the "sandwich ELISA" results using different nanozymes and natural enzyme HRP.

E. coli O157:H7 recoveries were identified in real-world complex food samples such as milk and spinach to further show the robust and field-deployable detection capabilities of our MPnS-based "sandwich ELISA" colorimetric test in the agrifood business **(Figure 25)**. While the milk sample's sensitivity was significantly reduced due to the presence of milk-based higher molecular weight proteins, bacterial CFUs were identified at concentrations as low as 10^3. The MPnS, on the other

hand, demonstrated a greater sensitivity, identifying CFUs at concentrations of 10^2 in spiked spinach samples. This might be owing to smaller molecular weight natural product interferences in spinach washing. These sensitive detection results support our prediction that the MPnS nanozyme may be utilized successfully in field applications to detect *E. coli* O157:H7 at low concentration levels. Because of the low infection incidence of these bacterium in food and drinking sources, this discovery is important. Furthermore, because of our platform's flexibility, the MPnS-based "sandwich ELISA" test may be easily modified to detect a wide range of pathogens, including viruses.

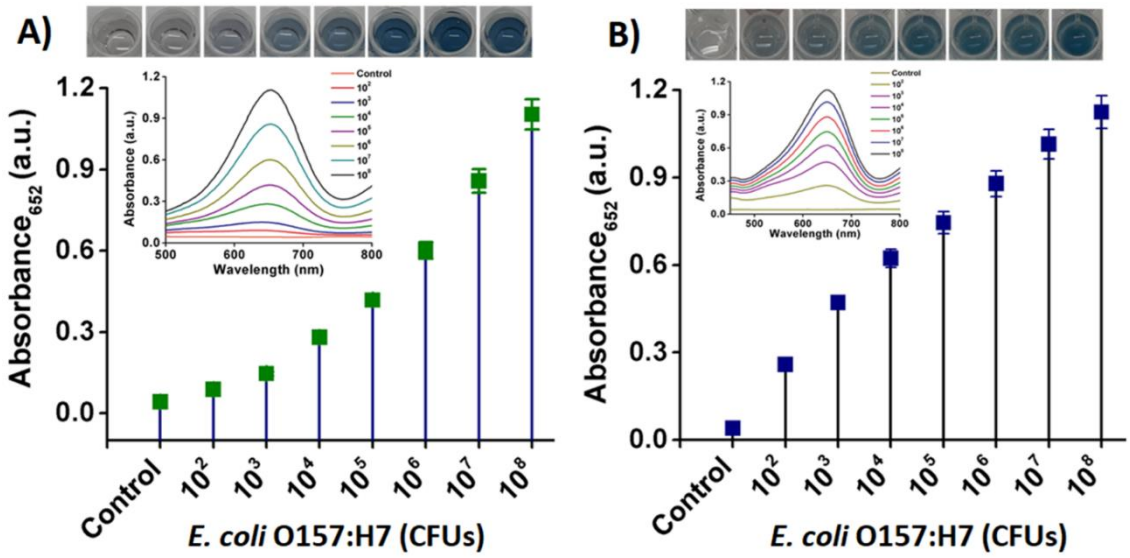

Figure 25: Colorimetric detection of different CFUs of *E.coli O157:H7* spiked in (A) milk and (B) spinach rinse using MPnS in "sandwich ELISA" format. The absorbance of TMB at 652 nm was plotted as a function of different CFUs of bacteria.

9. Specific and Rapid Detection of *E. coli* O157:H7

To further mimic real-world capability of MPnS nanozyme, we used UV absorbance and colorimetry to demonstrate the specificity of our platform for *E. coli* O157:H7 in the presence of other pathogenic contaminants, including *S. Typhimurium* and another *E. coli* strain, specifically *E. coli O111* (**Figure 26A-B**). While the interaction of *S. Typhimurium* was almost as minimal as that of control, *E. coli O111* demonstrated slight reactivity with the MPnS-Ab, but not enough to be visible to the naked eye. However, high specificity for *E. coli* O157:H7 was demonstrated with an

intense color change in response to the *E. coli* O157:H7 in sample, which was also clearly observed by UV absorbance.

In addition to rapid assay, we employed time-dependent assays to show that our platform can be used for quick *E. coli* O157:H7 testing. We began with HRP, which demands high bacterial CFUs and demonstrated optimal performance with CFUs magnitudes of 10^7 and detection signals lasting longer than 30 min **(Figure 26C)**. This was predicted because HRP is utilized in the conventional ELISA assay, where it begins to change color after around 20 to 30 minutes.

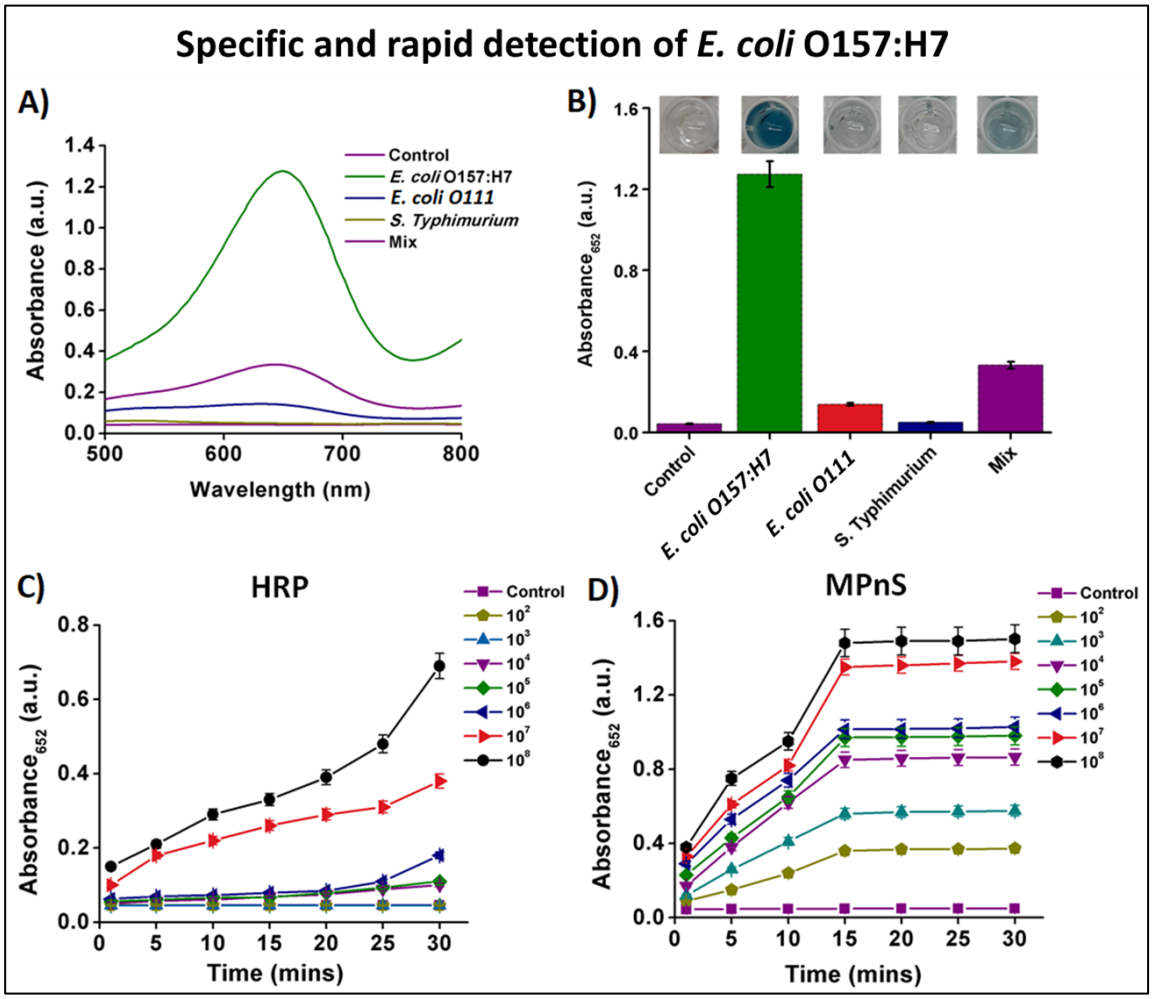

Figure 26: (A and B) Specificity of MPnS was evaluated by conducting MPnS-based sandwich ELISA in the presence of other bacterial cross-contaminants and a mixture. (C and D) Time-dependent *E. coli* O157:H7 detection assay using (C) HRP and (D) MPnS.

When compared to HRP, the peroxidase mimetic MPnS exhibited detection capabilities starting at concentrations as low as 10^3 and a detection period of 15 minutes **(Figure 26D).** We reasoned that the synergistic effects of GNPs and IONPs increased sensitivity and detection time, resulting in faster readings with a steady signal within 10 to 15 minutes and outperforming the conventional ELISA test. This demonstrates that our MPnS trimodal detection method can be utilized on-site to identify *E. coli* O157: H7 in real-time, with high sensitivity and less detection time.

Chapter III

Experimental Section

1. Materials

Ferric chloride ($FeCl_3.6H_2O$), ferrous chloride ($FeCl_2.4H_2O$), ammonium hydroxide (NH_4OH), hydrochloric acid (HCl) were obtained from Fisher Scientific, ACS reagent grade. 1-ethyl-3-(3-(dimethylamino) propylcarbodimide hydrochloride (EDC), *N*-hydroxysuccinimide (NHS), polyacrylic acid (PAA), Hydrogen tetrachloroaurate (III) hydrate ($HAuCl_4.3H_2O$), sodium citrate (NaCit), 2-morpholinoethanesulfonic acid (MES), 3,3',5,5'-Tetramethylbenzidine (TMB), hydrogen peroxide 30% (H_2O_2), horse radish peroxidase (HRP), phosphate buffer saline (PBS) was obtained from Sigma-Aldrich. Bacterial strains *E. coli* O157:H7, staphylococcus aureus, generic *E. coli* were purchased from American Type Culture Collection (ATCC). Nutrient agar, nutrient broth, ELISA washing buffer/coating buffer were purchased from Fisher. Anti-*E. coli* O157:H7 antibody and Conjugation Check & Go Kit were obtained from Abcam. The dialysis bag (MWCO 6–8 K) was purchased from Spectrum Labs. All the glassware was used after autoclave.

2. Instrumentation

Size and zeta potential of nanozymes (IONPs, GNP and MPnS) were measured using Malvern's Zetasizer-ZS90. A Tecan i-control infinite M200 plate reader was used for the measurement of absorbance. Type-1 de-ionized (DI) water (18.2 MΩxcm at 25 o C) was obtained using GenPure UV-TOC from Thermo Scientific. Kinetics studies were performed on a Genesys 150 Spectrophotometer.

3. Synthesis of Gold Nanoparticles (GNPs)

In order to synthesize GNPs, 5 mM $HAuCl_4$ (2.0 mL) (21 mg in 12.5 mL in DI water) was added into DI water (17 mL) at 95 °C in 50 mL Erlenmeyer flask placed on a hot plate with a magnetic stir bar. After boiling for 10 min, 0.5% NaCit (1.0 mL) (5 mg in 1 mL DI water) was added into the reaction mixture, with continue stirring and heating. The reaction continued for 20 min until a ruby red color was observed. The resulting solution was purified by dialysis (MWCO: 6–8 K) in water to remove unreacted particles and GNPs were stored at 4 °C. The average diameter of these GNPs was found to be 18±2 nm.

4. Synthesis of Iron Oxide Nanoparticles (IONPs)

The IONPs were synthesized by the water precipitation method following our previously reported method. Briefly, 3 solutions were made. Solution 1 contained $FeCl_3$ (0.622 g), $FeCl_2$ (0.334 g), and H_2O (2 mL). Solution 2 contained NH_4OH (1.8 mL of 30% stock) and H_2O (15 mL). The solution 3 contained polyacrylic acid (0.859 g) and H_2O (5 mL). After preparing all the solutions HCl (90 uL 12M) was added to solution 1, and then solution 1 was added to solution 2 in vortexing condition at 875 RPM. Immediately within 9 sec solution 3 was added into solution 2 in vertexing condition. Vortexing continued the mixture at 3000 RPM for 1 h. After the mixing, the solution was centrifuged for 20 min at 1,620 x g and then 20 min at 2,880 x g to remove the larger particles. The supernatant was collected and dialyzed (molecular weight cutoff: 6–8 K) in water overnight to remove unreacted mixture. The purified IONPs were stored at room temperature. The average diameter of these IONPs was found to be 91±2 nm.

5. Synthesis of Magneto Plasmonic Nanoparticles (MPnS)

To synthesize MPnS, 5 mM $HAuCl_4$ (2.0 mL) (21 mg in 12.5 mL in DI water) was added to IONPs (T2= 100-110 mSec) (17.0 mL) diluted in DI water in a 50 mL Erlenmeyer flask. The flask was placed on a hot plate and stirred at 500 RPM at 95 °C. After boiling for 10 mins, 0.5% NaCit (1.0 mL) (5 mg in 1 mL DI water) was added to the reaction mixture, with continued stirring and heating. The reaction continued for 20 min until a dark purple color was observed. The nanoparticles were

purified by Magnetic column and stored at 4 °C. The average diameter of these MPnS was found to be 68±2 nm.

6. Synthesis of MPnS-mAb

Prior to the conjugation to MPnS, the pH of MPnS was adjusted at 9.0 using 150 mM potassium carbonate. A MPnS solution with OD520 = 1.0 (250 μL portions) was added to solutions containing 15 μL PBS (1 X, pH 7.5) with antibodies (mAb) in concentrations from 0.5 to 16 μg. The mixture was vortexed and incubated for 10 min on rotator with continuous vortexing. Then 50 μL of 10% NaCl was added in 50 μL of each conjugate and incubated for another 10 min. The absorbance was measured at 580 nm. Then a flocculation curve was plotted as dependences of the OD580 nm in the presence of excess salt (10% NaCl) versus the antibody concentration. To synthesize MPnS-mAb conjugates, antibodies at selected concentrations (8 μg) were mixed with the MPnS solution. The mixture was incubated with stirring at room temperature for 30 min, and BSA was added to final concentration of 1% (25 μL of 10% BSA was added in total 250 μL of MPnS-mAb conjugate) and incubated for another 30 min. The unbound antibodies and BSA were removed by centrifugation at 3000 rpm for 5 min. The supernatant was removed, and the pellet was resuspended in a conjugation buffer containing 10 mM Tris-HCl buffer (pH 9.0) and 0.5% BSA. The spectra of the MPnS and their conjugate were recorded with a Tecan i-control infinite M200 plate reader.

7. Bacterial Culture

Freeze dried pellet of *E. coli* O157:H7 strain were obtained from ATCC. Pellets were hydrated into 5 mL of nutrient broth media. Using the spread plate method, 100 μL of this solution was spread onto an agar plate using a L-shaped glass spreader and incubated for 24 h at 37^{o} C. An isolated colony was inoculated into 35 mL of nutrient broth in a 250 mL of flask. The sample was incubated overnight at 37^{o} C with 200 rpm agitation. The bacterial solution was centrifuged at 6000xg rpm for 2 minutes, and the pellets were washed with 1X PBS (7.5 pH) twice. Finally, the optical density of the solution was adjusted at 0.1 in PBS, which gives a stock solution of 10^{-8} bacterial CFUs in the solution. Different dilutions were made for different concentrations. Conformation of the bacterial concentration in the solution was obtained by plating on an agar plate.

8. Kinetic Analysis

Catalytic activity of HRP, IONP, GNP, and MPnS were determined at room temperature in a 4.5 mL cuvette using 20 pM HRP, 0.9 pM IONP, 0.6 pM GNP and 0.2 pM MPnS in the presence of 10 mM, 980 mM, 210 mM, and 210 mM H_20_2 respectively, and TMB was added as a substrate. As we increased the TMB concentration, the nanozyme activity also increased which gives a non-linear curve. Using this graph, a Michaelis-Menten graph was obtained using Origin Pro 2019 with the Michaelis-Menten enzyme kinetic model.

All reactions were measured using a Genesys 150 Spectrophotometer with the kinetics method at 652 nm. The maximum initial velocity (V_{max}), Michaelis-Menten constant (K_m) and catalytic constant (K_{cat}) were determined for all enzymes.

9. Peroxidase like activity of nanozymes

The enzymatic activity of nanozymes is depends on the concentrations of TMB, H_20_2, pH, and temperature. We measured the catalytic activity of nanozymes at 0 to 1 M H_20_2 concentration, 1 to 9 pH, 20^o C to 60^o C temperature and different size of nanomaterials. We compared the relative enzymatic activity of GNP, IONP and MPnS with the conventional enzyme HRP. Using a Tecan i-control infinite M200 plate reader, the reaction was measured at 652 nm wavelength.

10. Sandwich Immunoassay

The 96 well microplate was coated with the 200 µL of anti-*E. coli* o157:H7 capture antibody (0.1 mg/mL) (A15Z (MA5-97)) in a coating buffer overnight at 4^o C. After the incubation, the plate was washed three times with washing buffer without disturbing the layer of capture antibody. The wells were blocked using blocking buffer for 2 hrs at 37^0 C and washed three times with washing buffer. In each well different CFUs of *E. coli* O157:H7 were added and incubated for 2 hrs at 37^0 C. Unbound CFUs were removed with washing buffer three times. MPnS-ab (anti-*E. coli* 0157:H7 antibody conjugated MPnS) was added to each well for 2 hrs at room temperature. The wells were washed three times with washing buffer. 100 µL of PBS (1X, 7.4 pH), 800 µM TMB and 210 mM H_20_2 were added to each well and incubated for 10 mins. Absorbance was measured using a Tecan i-control infinite M200 plate reader, and photographs were taken with iPhone 12 smart phone. For

comparison, HRP-based conventional ELISA, GNP-Ab and IONP-Ab based ELISA were performed.

11. Specificity Assay

For the confirmation of the specificity of the assay, sandwich ELISA was performed using CFUs of different pathogens *E. coli* O157:H7, *E. coli* O111, *S. Typhimurium,* and a mixed culture of these pathogens. The capture and detection antibody are specific to *E. coli* O157:H7, so there was no or minimal binding with the other pathogens.

12. Sandwich ELISA in real sample

Detection of pathogens in real sample such as milk and spinach rinse using MPnS-Ab was carried out. Milk was spiked with *E. coli* 0157:H7 CFUs and diluted as desired CFUs in the sample. The spinach rinse water was spiked with the *E. coli* 0157:H7 CFUs and culture diluted as required for desired CFUs. The similar protocol was used as sandwich immunoassay.

Chapter IV

Conclusion and Future Study

In brief, we have demonstrated successful synthesis of MPnS with integrated plasmonic and peroxidase-mimetic properties. Our results suggest that MPnS exhibited higher detection sensitivity than the natural enzyme and standalone nanomaterials. This was attributed to its superior catalytic activity ($k_{cat} \sim 10^5$) due to the synergistic peroxidase-mimetic activity of iron and several encapsulated gold nanoparticles. MPnS enabled ELISA exhibits lower turnaround time than conventional ELISA. We were successfully able to detect the pathogen in real food matrices such as milk and spinach rinse. Formulated MPnS is customizable and can be tailored for the detection of other food borne pathogens.

In the future, we are planning to put this nanozyme platform in a lateral flow assay using the plasmonic property of MPnS, and we will further investigate the translatability of catalytic activity of MPnS technology in LFA platform.

References

Chapter I

1. https://www.cdc.gov/foodsafety/foodborne-germs.html
2. https://ndc.services.cdc.gov/case-definitions/shiga-toxin-producing-escherichia-coli-2018/
3. Gally, D. L.; Stevens, M. P. Microbe Profile: *Escherichia coli* O157: H7 – notorious relative of the microbiologist's workhorse. *Microbiology* **2007**, 163, 1-3, doi: 10.1099/mic.0.000387.
4. Lim, J. Y.; Yoon, J.; Hovde, C. J.; A brief overview of *Escherichia coli* O157:H7 and its plasmid O157. *J Microbiol Biotechnol* **2010**, 20 (1), 5-14.
5. Gibson, G. R.; Macfarlane, G. T.; eds. Conway PL: Microbial ecology of the human large intestine. In Human Colonic Bacteria: Role in Nutrition, Physiology, and Pathology. Boca Raton, FL, CRC Press, **1995**, pp 1-24.
6. Escherich, T. Die darmbakterien des neugeborenen und sauglings. *Fortshr. Med.* **1885**, **3, 5**15-522.
7. Mainil, J. Escherichia coli virulence factors. *Vet Immunol Immunopathol* **2013**, 152(1-2), 2-12, doi: 10.1016/j.vetimm.2012.09.032.
8. https://biosciencenotes.com/e-coli-background-classification-cultural-and-biochemical-characters-virulence-factors/
9. Cabeen MT, Jacobs-Wagner C. Bacterial cell shape. Nat Rev Microbiol. **2005**, 8, 601-610. doi: 10.1038/nrmicro1205.
10. Matias VR, Al-Amoudi A, Dubochet J, Beveridge TJ. Cryo-transmission electron microscopy of frozen-hydrated sections of Escherichia coli and Pseudomonas aeruginosa. *J Bacteriol*. **2003,** 5(20), 6112-6118, doi: 10.1128/JB.185.20.6112-6118.2003.
11. Kellenberger, E.; Ryter, A. Cell wall and cytoplasmic membrane of Escherichia coli. *J Biophys Biochem Cytol*. **1958**, 4(3), 323-326, doi: 10.1083/jcb.4.3.323.
12. Rogers HJ: Bacterial Cell Structure. American Society for Microbiology, Washington, D.C., **1983**
13. http://www.rocketswag.com/culinary/food-poisoning/Structure-And-Function-Of-A-Ecoli-Bacteria.
14. Terashima H, Kojima S, Homma M. Flagellar motility in bacteria structure and function of flagellar motor. *Int Rev Cell Mol Biol 270* **2008**, 39–85. doi:10.1016/s1937-6448(08)01402-0.

15. Jayappa HG, Goodnow RA, Geary SJ. Role of Escherichia coli type 1 pilus in colonization of porcine ileum and its protective nature as a vaccine antigen in controlling colibacillosis. *Infect Immun*. **1985**, 48(2), 350-354, doi: 10.1128/iai.48.2.350-354.1985.
16. https://www.itis.gov/servlet/SingleRpt/SingleRpt?search_topic=TSN&search_value=285#null
17. https://www.cram.com/essay/Classification-Of-Escherichia-Coli/F3RT235KUYKQ#google_vignette
18. https://sites.google.com/site/cwibiolfrankjmcmillanpbl/phylogenetic-tree-of-e-coli
19. http://ymbiodelaramdescherichiacoli.weebly.com/habitat.html
20. http://bioweb.uwlax.edu/bio203/s2013/champa_hail/habitat.htm
21. Alon, U.; Surette, M.G.; Barkai, N.; Leibler, S. Robustness in bacterial chemotaxis. *Nature* **1999**, 397, 168–171, doi: 10.1038/16483
22. https://www.slideshare.net/MMASSY/e-coli-lectur-revised-alpana
23. Fratamico, P. M.; DebRoy, C.; Liu, Y.; Needleman, D. S.; Baranzoni, G. M.; Feng, P. Advances in Molecular Serotyping and Subtyping of Escherichia coli. *Front Microbiol*. **2016**, 3,7,644. doi: 10.3389/fmicb.2016.00644.
24. Sarkar, S.; Ulett, G. C.; Totsika, M.; Phan, M.-D.; Schembri, M. A. Role of capsule and O antigen in the virulence of uropathogenic *Escherichia coli*. *PLoS ONE* **2014**, 9:e94786. doi: 10.1371/journal.pone.0094786
25. https://www.slideshare.net/MMASSY/e-coli-lectur-revised-alpana
26. James, H. J.; Michael, A. P. *Manual of Clinical microbiology*. **2015**, Washington, DC: ASM Press. 11th Edition ISBN 9781555817374.
27. Sowers, E. G.; Wells, J. G.; Strockbine, N. A. Evaluation of commercial latex reagents for identification of O157 and H7 antigens of Escherichia coli. *J Clin Microbiol*. **1996**, 34(5), 1286-1289, doi: 10.1128/jcm.34.5.1286-1289.1996.
28. Fields, P. I.; Blom, K.; Hughes, H. J.; Helsel, L. O.; Feng, P.; Swaminathan, B. Molecular characterization of the gene encoding H antigen in Escherichia coli and development of a PCR-restriction fragment length polymorphism test for identification of *E. coli* O157:H7 and O157:NM. *J Clin Microbiol*. **1997**, 35(5), 1066-1070, doi: 10.1128/jcm.35.5.1066-1070.1997.
29. CDC *E. coli* Factsheet. https://www.cdc.gov/ecoli/pdfs/CDC-E.-coli-Factsheet.pdf
30. https://www.cdc.gov/ecoli/ecoli-symptoms.html

31. Rangel, J. M.; Sparling, P. H.; Crowe, C.; Griffin, P. M.; Swerdlow, D. L. Epidemiology of Escherichia coli O157:H7 Outbreaks, United States, 1982–2002. *Emerging Infectious Diseases* **2005**,11(4), 603-609, doi: 10.3201/eid1104.040739.
32. http://www.fao.org/fileadmin/user_upload/fcc/news/1_FAO_Preventing-E.Coli-inFood_FCC_2011.06.23.pdf
33. https://www.cdc.gov/ecoli/outbreaks.html
34. Deisingh, A. K.; Thompson, M. Strategies for the detection of Escherichia coli O157:H7 in foods. *Journal of applied microbiology* **2004**, 96, 419-429, doi: 10.1111/j.1365-2672.2003.02170.x.
35. March, S. B.; Ratnam, S. Sorbitol-MacConkey medium for detection of Escherichia coli O157:H7 associated with hemorrhagic colitis. *J Clin Microbiol* **1986**, 23, 869-872, doi: 10.1128/jcm.23.5.869-872.1986
36. O'Sullivan, J.; Bolton, D. J.; Duffy, G.; Baylis, C.; Tozzoli, R.; Wasteson Y.; Lofdahl, S. Methods for Detection and Molecular Characterisation of Pathogenic Escherichia coli, **2008**, ISBN 1 84170 506 3, T Dublin.
37. Bopp, C. A.; Brenner, F. W.; Fields, P. I.; Wells, J. G.; Strockbine, N. A. *Escherichia, Shigella*, and *Salmonella*. In: Murray PR, Baron EJ, Jorgensen JH, Pfaller MA, Yolken RH, Eds. *Manual of Clinical Microbiology* **2003,** 8 Washington, DC, ASM Press.
38. Atkinson, R. B.; Besser, J. B. ; Bopp, C. A. ; Carlson, C. ; Crandall, C. ; George, K.; Gerner-Smidt, P.; Gladbach, S.; Gould, L. H.; Hartley, C. S.; Maguire, H.; Monson, T. A.; Rutledge, D.; Shea, S.; Somsel, P. A.; Strockbine, N. A. Guidance for Public Health Laboratories on the Isolation and Characterization of Shiga toxin-producing Escherichia coli (STEC) from Clinical Specimens. **2012**.
39. Safarik, I.; Safarikova, M.; Forsythe, S. J. The application of magnetic separation in applied microbiology. *Journal of Applied Bacteriology* **1995**, 78, 575–585, doi: 10.1111/j.1365-2672.1995.tb03102.x.
40. https://wonder.cdc.gov/wonder/prevguid/p0000445/p0000445.asp#head003000000000000
41. Yoshitomi, K. J.; Jinneman, K. C.; Zapata, R.; Weagant, S. D.; Fedio, W. M. Detection and isolation of low levels of *E. coli* O157:H7 in cilantro by real-time PCR, immunomagnetic separation, and cultural methods with and without an acid treatment. *J Food Sci*. **2012**, 77(8), M481-9, doi: 10.1111/j.1750-3841.2012.02813.x.
42. Wei, T.; Du, D.; Zhu, M. J.; Lin, Y.; Dai, Z. An Improved Ultrasensitive Enzyme-Linked Immunosorbent Assay Using Hydrangea-Like Antibody-Enzyme-Inorganic Three-in-One

Nanocomposites. *ACS Appl Mater Interfaces* **2018**, 8(10), 6329-6335, doi: 10.1021/acsami.5b11834.

43. Stryer, L.; Berg, J. M.; Tymoczko, J. L. Biochemistry **2002** (5) San Francisco: W.H. Freeman. ISBN 0-7167-4955-6.
44. Shan, S.; Liu, D.; Guo, Q.; Wu, S.; Chen, R.; Luo, K.; Hu, L.; Xiong, Y.; Lai, W. Sensitive detection of Escherichia coli O157:H7 based on cascade signal amplification in ELISA. *J Dairy Sci.* **2016**, 99(9), 7025-7032, doi: 10.3168/jds.2016-11320.
45. Malou, N.; Raoult, D. Immuno-PCR: a promising ultrasensitive diagnostic method to detect antigens and antibodies. *Trends Microbiol.* **2011**, 19(6), 295-302. doi: 10.1016/j.tim.2011.03.004.
46. Gould, E. A.; Buckley, A.; Cammack, N. Use of the biotin-streptavidin interaction to improve flavivirus detection by immunofluorescence and ELISA tests. *J Virol Methods* **1985**, 11(1), 41-48, doi: 10.1016/0166-0934(85)90123-5.
47. Chen, R.; Huang, X.; Xu, H.; Xiong, Y.; Li, Y. Plasmonic Enzyme-Linked Immunosorbent Assay Using Nanospherical Brushes as a Catalase Container for Colorimetric Detection of Ultralow Concentrations of Listeria monocytogenes. *ACS Appl Mater Interfaces* 2015, 7(51), 28632-28639, doi: 10.1021/acsami.5b10181.
48. Su, H.; Zhao, H.; Qiao, F.; Chen, L.; Duan, R.; Ai, S. Colorimetric detection of Escherichia coli O157:H7 using functionalized Au@Pt nanoparticles as peroxidase mimetics. *Analyst*. **2013**, 138(10), 3026-3031, doi: 10.1039/c3an00026e.
49. https://starfishmedical.com/blog/best-method-detect-e-coli/
50. Newton, C. R.; Graham, A. PCR, **1997**, 2nd edn. Oxford: Bios Scientific.
51. Livak, K. J. Quantitation of DNA/RNA Using Real-time PCR Detection. **2002** http://www.appliedbiosystems.com/molecularbiology/about/pcr/sds/white.html.
52. Masdor, N.A.; Altintas, Z.; Tothill, I.E. Surface Plasmon Resonance Immunosensor for the Detection of *Campylobacter jejuni*. *Chemosensors* **2017**, *5*, 16, doi: 10.3390/chemosensors5020016.
53. Wang, Y.; Ye, Z.; Si, C.; Ying, Y. Monitoring of Escherichia coli O157:H7 in food samples using lectin based surface plasmon resonance biosensor. *Food Chem.* **2013**, 136(3-4), 1303-1308, doi: 10.1016/j.foodchem.2012.09.069.
54. Banerjee, T.; Sulthana, S.; Shelby, T.; Heckert, B.; Jewell, J.; Woody, K.; Karimnia, V.; McAfee, J.; Santra, S. Multiparametric Magneto-fluorescent Nanosensors for the Ultrasensitive Detection of Escherichia coli O157:H7. *ACS Infect Dis*. **2016**, 2(10), 667-673, doi: 10.1021/acsinfecdis.6b00108.

55. Gupta, R.; Kumar, A.; Kumar, S.; Pinnaka, A. K.; Singhal, N. K. Naked eye colorimetric detection of *Escherichia coli* using aptamer conjugated graphene oxide enclosed Gold nanoparticles. *Sensors and Actuators B: Chemical* **2021**, 129100, doi: 10.1016/j.snb.2020.129100.

Chapter II

1. Centers for Disease Control and Prevention. (n.d.). Preliminary Incidence and Trends of Infections with Pathogens Transmitted Commonly Through Food — *Foodborne Diseases Active Surveillance Network*, 10 U.S. Sites, 2015–2018. CDC. Retrieved January 25, **2021**, from https://www.cdc.gov/mmwr/volumes/68/wr/mm6816a2.htm?s_cid=mm6816a2_w
2. Estimates of Foodborne Illness in the United States. (**2019**). CDC. https://www.cdc.gov/foodborneburden/index.html
3. BYRNE, L.; JENKINS, C.; LAUNDERS, N.; ELSON, R.; ADAK, G. K. The epidemiology, microbiology, and clinical impact of Shiga toxin-producing Escherichia coli England 2009–2012. *Epidemiology and Infection*. **2015**, *143*(16), 3475–3487.
4. Nyachuba, D. G. Foodborne illness: is it on the rise? *Nutrition Reviews*. **2010**, *68*(5), 257–269.
5. BEUCHAT, L. R. Pathogenic Microorganisms Associated with Fresh Produce. *Journal of Food Protection*. **1996**, *59*(2), 204–216.
6. Adams, N. L.; Byrne, L.; Smith, G. A.; Elson, R.; Harris, J. P; Salmon, R.; Smith, R.; O'Brien, S. J.; Adak, G. K.; Jenkins, C. Shiga Toxin–Producing Escherichia coli O157, England and Wales, 1983–2012. *Emerging Infectious Diseases*. **2016**, *22*(4), 590–597.
7. Jung, Y.; Jang, H.; Matthews, K. R. Effect of the food production chain from farm practices to vegetable processing on outbreak incidence. *Microbial Biotechnology*. **2014**, *7*(6), 517–527.
8. Mikhail, A. F. W.; Jenkins, C.; Dallman, T. J.; Inns, T.; Douglas, A.; Martín, A. I. C.; Fox, A.; Cleary, P.; Elson, R.; Hawker, J. An outbreak of Shiga Toxin-producing Escherichia coli O157:H7 associated with contaminated salad leaves: epidemiological, genomic and food trace back investigations – CORRIGENDUM. *Epidemiology and Infection*. **2018**, *146*(14),1879–1879.
9. Centers for Disease Control and Prevention. Outbreak of *E. coli* Infections Linked to Leafy Greens. Available from: https://www.cdc.gov/ecoli/2020/o157h7-10-20b/index.html. Accessed January 25 2021

10. U.S Food and Drug Administration. Outbreak Investigation of *E. coli* O157:H7: Unknown Food (Fall 2020). Available from: https://www.fda.gov/food/outbreaks-foodborne-illness/outbreak-investigation-e-coli-o157h7-unknown-food-fall-2020. Accessed January 25, **2021**.
11. Pires, S. M.; Majowicz, S.; Gill, A.; Devleesschauwer, B. Global and regional source attribution of Shiga toxin-producing Escherichia coli infections using analysis of outbreak surveillance data. *Epidemiology and infection*. **2019**, *147*, e236.
12. Griffin, P. M.; Tauxe, R. V. The Epidemiology of Infections Caused by Escherichia coli O157: H7, Other Enterohemorrhagic *E. coli*, and the Associated Hemolytic Uremic Syndrome. *Epidemiologic Reviews*. **1991**, *13*(1), 60–98.
13. Gyles, C. L. Escherichia coli cytotoxins and enterotoxins. *Canadian Journal of Microbiology*. **1992**, *38*(7), 734–746.
14. Ito, H.; Terai, A.; Kurazono, H.; Takeda, Y.; Nishibuchi, M. Cloning and nucleotide sequencing of Vero toxin 2 variant genes from Escherichia coli O91: H21 isolated from a patient with the hemolytic uremic syndrome. *Microbial Pathogenesis*. **1990**, *8*(1), 47–60.
15. Wang, G.; Clark, C. G.; Rodgers, F. G. Detection in Escherichia coli of the Genes Encoding the Major Virulence Factors, the Genes Defining the O157:H7 Serotype, and Components of the Type 2 Shiga Toxin Family by Multiplex PCR. *Journal of Clinical Microbiology*. **2002**, *40*(10), 3613–3619.
16. Reinthaler, F. F.; Galler, H.; Feierl, G.; Haas, D.; Leitner, E.; Mascher, F.; Melkes, A.; Posch, J.; Pertschy, B.; Winter, I.; Himmel, W.; Marth, E.; Zarfel, G. Resistance patterns of Escherichia coli isolated from sewage sludge in comparison with those isolated from human patients in 2000 and 2009. *Journal of Water and Health*. **2012**, *11*(1), 13–20.
17. Sun, H.; Zhang, H.; Ang, E. L.; Zhao, H. Biocatalysis for the synthesis of pharmaceuticals and pharmaceutical intermediates. *Bioorganic & Medicinal Chemistry*. **2018**, *26*(7), 1275–1284.
18. Patel, R. N. Biocatalysis for synthesis of pharmaceuticals. *Bioorganic & Medicinal Chemistry*. **2018**, *26*(7), 1252–1274.
19. Huisman, G. W.; Collier, S. J. On the development of new biocatalytic processes for practical pharmaceutical synthesis. *Current Opinion in Chemical Biology*. **2013**, *17*(2), 284–292.
20. Panesar, P. S.; Kumari, S.; Panesar, R. Biotechnological approaches for the production of prebiotics and their potential applications. *Critical Reviews in Biotechnology*. **2012**, *33*(4), 345–364.

21. Fernandes, P. Enzymes in Food Processing: A Condensed Overview on Strategies for Better Biocatalysts. *Enzyme Research*, **2010**, *2010*, 1–19.
22. Akoh, C. C.; Chang, S. W.; Lee, G. C.; Shaw, J. F. Biocatalysis for the Production of Industrial Products and Functional Foods from Rice and Other Agricultural Produce. *Journal of Agricultural and Food Chemistry*, **2008**, *56*(22), 10445–10451.
23. Kapoor, S.; Rafiq, A.; Sharma, S. Protein engineering and its applications in food industry. *Critical Reviews in Food Science and Nutrition*, **2015**, *57*(11), 2321–2329.
24. Hemalatha, T.; UmaMaheswari, T.; Krithiga, G.; Sankaranarayanan, P.; Puvanakrishnan, R. Enzymes in clinical medicine: an overview. *Indian J Exp Biol*. **2013**, 51(10), 777-788.
25. Sun, D. W. (Ed.). (2011). *Handbook of Food Safety Engineering*. Wiley-Blackwell. https://doi.org/10.1002/9781444355321
26. Huang, L. ; Sun, D. ; Pu, H. ; Wei, Q. Development of Nanozymes for Food Quality and Safety Detection: Principles and Recent Applications. *Comprehensive Reviews in Food Science and Food Safety*, **2019**, *18*(5), 1496–1513.
27. Meunier, B. ; de Visser, S. P. ; Shaik, S. Mechanism of Oxidation Reactions Catalyzed by Cytochrome P450 Enzymes. *Chemical Reviews*. **2004**, *104*(9), 3947–3980.
28. Kirby, A. J. Efficiency of Proton Transfer Catalysis in Models and Enzymes†. *Accounts of Chemical Research*. **1997**, *30*(7), 290–296.
29. Wang, X. Y.; Guo, W. J.; Hu, Y. H.; Wu, J. J.; Wei, H. Nanozymes: Next Wave of Artificial Enzymes. *Springer*. **2016**.
30. Yan, X. Y. Nanozyme: a new type of artificial enzyme. *Prog. Biochem. Biophys.* **2018**, 45, 101−104.
31. Gao, L.; Zhuang, J.; Nie, L.; Zhang, J.; Zhang, Y.; Gu, N.; Wang, T.; Feng, J.; Yang, D.; Perrett, S.; Yan, X. Intrinsic peroxidase-like activity of ferromagnetic nanoparticles. *Nature Nanotechnology*. **2007**, *2*(9), 577–583.
32. Breslow, R. Artificial Enzymes. Wiley-VCH. Weinheim, **2005**.
33. Ali, S. S.; Hardt, J. I.; Quick, K. L.; Sook Kim-Han, J.; Erlanger, B. F.; Huang, T.; Epstein, C. J.; Dugan, L. L. A biologically effective fullerene (C60) derivative with superoxide dismutase mimetic properties. *Free Radical Biology and Medicine*. **2004**, *37*(8), 1191–1202.
34. Kataky, R.; Morgan, E. Potential of enzyme mimics in biomimetic sensors: a modified-cyclodextrin as a dehydrogenase enzyme mimic. *Biosensors and Bioelectronics*. **2003**, *18*(11), 1407–1417.

35. Kirkorian, K.; Ellis, A.; Twyman, L. J. Catalytic hyperbranched polymers as enzyme mimics; exploiting the principles of encapsulation and supramolecular chemistry. *Chemical Society Reviews*. **2012**, *41*(18), 6138.
36. Liu, L.; Breslow, R. Dendrimeric Pyridoxamine Enzyme Mimics. *Journal of the American Chemical Society*. **2003**, *125*(40), 12110–12111.
37. Anderson, H. L.; Sanders, J. K. M. Enzyme mimics based on cyclic porphyrin oligomers: strategy, design and exploratory synthesis. *Journal of the Chemical Society, Perkin Transactions 1*. **1995**, *18*, 2223-2229.
38. Romanovsky, B. V. Transition metal complexes in inorganic polymers as enzyme mimics. *Macromolecular Symposia*. **1994**, *80*(1), 185–192.
39. Gong, L.; Zhao, Z.; Lv, Y. F.; Huan, S. Y.; Fu, T.; Zhang, X. B.; Shen, G. L.; Yu, R. Q. DNAzyme-based biosensors and nanodevices. *Chemical Communications*. **2015**, *51*(6), 979–995.
40. Jiang, B.; Duan, D.; Gao, L.; Zhou, M.; Fan, K.; Tang, Y.; Xi, J.; Bi, Y.; Tong, Z.; Gao, G. F.; Xie, N.; Tang, A.; Nie, G.; Liang, M.; & Yan, X. Standardized assays for determining the catalytic activity and kinetics of peroxidase-like nanozymes. *Nature Protocols*. **2018**, *13*(7), 1506–1520.
41. Wang, P.; Wang, T.; Hong, J.; Yan, X.; Liang, M. Nanozymes: A New Disease Imaging Strategy. *Frontiers in Bioengineering and Biotechnology*. **2020**, *8*.
42. Huang, Y.; Ren, J.; Qu, X. Nanozymes: Classification, Catalytic Mechanisms, Activity Regulation, and Applications. *Chemical Reviews*. **2019**, *119*(6), 4357–4412.
43. Huang, L. ; Sun, D. ; Pu, H. ; Wei, Q. Development of Nanozymes for Food Quality and Safety Detection: Principles and Recent Applications. *Comprehensive Reviews in Food Science and Food Safety*. **2019**, *18*(5), 1496–1513.
44. Wang, X.; Hu, Y.; Wei, H. Nanozymes in bionanotechnology: from sensing to therapeutics and beyond. *Inorganic Chemistry Frontiers*. **2016**, *3*(1), 41–60.
45. He, W.; Wamer, W.; Xia, Q.; Yin, J.; Fu, P. P. Enzyme-Like Activity of Nanomaterials. *Journal of Environmental Science and Health, Part C*. **2014**, *32*(2), 186–211.
46. Karakoti, A.; Singh, S.; Dowding, J. M.; Seal, S.; Self, W. T. Redox-active radical scavenging nanomaterials. *Chemical Society Reviews*. **2010**, *39*(11), 4422.

47. Pirmohamed, T.; Dowding, J. M.; Singh, S.; Wasserman, B.; Heckert, E.; Karakoti, A. S.; King, J. E. S.; Seal, S.; Self, W. T. Nanoceria exhibit redox state-dependent catalase mimetic activity. *Chemical Communications*. **2010**, *46*(16), 2736.
48. Singh, S. Cerium oxide based nanozymes: Redox phenomenon at biointerfaces. *Biointerphases*. **2016**, *11*(4), 04B202.
49. Karim, Md. N.; Anderson, S. R.; Singh, S.; Ramanathan, R.; Bansal, V. Nanostructured silver fabric as a free-standing Nanozyme for colorimetric detection of glucose in urine. *Biosensors and Bioelectronics*. **2018**, *110*, 8–15.
50. Zhang, H.; Liang, X.; Han, L.; Li, F. "Non-Naked" Gold with Glucose Oxidase-Like Activity: A Nanozyme for Tandem Catalysis. *Small*. **2018**, *14*(44), 1803256.
51. Zhao, M.; Tao, Y.; Huang, W.; He, Y. Reversible pH switchable oxidase-like activities of MnO2 nanosheets for a visual molecular majority logic gate. *Physical Chemistry Chemical Physics*. **2018**, *20*(45), 28644–28648.
52. Singh, S. Nanomaterials Exhibiting Enzyme-Like Properties (Nanozymes): Current Advances and Future Perspectives. *Frontiers in Chemistry*. **2019**, *7*.
53. Liang, M.; Yan, X. Nanozymes: From New Concepts, Mechanisms, and Standards to Applications. *Accounts of Chemical Research*. **2019**, *52*(8), 2190–2200.
54. Wei, H.; Wang, E. Nanomaterials with enzyme-like characteristics (nanozymes): next-generation artificial enzymes. *Chemical Society Reviews*. **2013**, *42*(14), 6060-6093.
55. Wu, J.; Wang, X.; Wang, Q.; Lou, Z.; Li, S.; Zhu, Y.; Qin, L.; Wei, H. Nanomaterials with enzyme-like characteristics (nanozymes): next-generation artificial enzymes (II). *Chemical Society Reviews*. **2019**, *48*(4), 1004–1076.
56. Santra, S.; Kaittanis, C.; Grimm J, Perez JM. Drug/dye-loaded, multifunctional iron oxide nanoparticles for combined targeted cancer therapy and dual optical/magnetic resonance imaging. Small. 2009;5(16):1862-8. doi: 10.1002/smll.200900389.
57. Kimling, J., Maier, M., Okenve, B., Kotaidis, V., Ballot, H., Plech, A. Turkevich Method for Gold Nanoparticle Synthesis Revisited. J. Phys. Chem. B. 2006;110;15700–07. PUBMED PMID:16898714 doi:10.1021/jp061667w
58. Banerjee T, Sulthana S, Shelby T, Heckert B, Jewell J, Woody K, et al. Multiparametric Magneto-fluorescent Nanosensors for the Ultrasensitive Detection of Escherichia coli O157:H7. ACS Infectious Diseases. 2016. doi: 10.1021/acsinfecdis.6b00108.

59. Herlet, J.; Kornberger, P.; Roessler, B.; Glanz, J.; Schwarz, W. H.; Liebl, W.; Zverlov, V. V. A new method to evaluate temperature vs. pH activity profiles for biotechnological relevant enzymes. *Biotechnology for Biofuels*. **2017**, *10*(1).
60. Xi, Z.; Gao, W.; Xia, X. Size Effect in Pd−Ir Core-Shell Nanoparticles as Nanozymes. *ChemBioChem*. **2020**, *21*(17), 2440–2444.